

1 **Microbiota-instructed regulatory T cell differentiation is mediated by a distinct ROR γ t⁺**
2 **antigen presenting cell subset**

3
4
5 Ranit Kedmi¹, Tariq Najar¹, Kailin R. Mesa¹, Allyssa Grayson^{1,2}, Lina Kroehling¹, Yuhan Hao^{3,4},
6 Stephanie Hao⁵, Maria Pokrovskii^{1,13}, Mo Xu^{1,14}, Jhimmy Talbot^{1,15}, Jiaxi Wang⁶, Joe Germino⁶,
7 Caleb A. Lareau⁷, Ansuman T. Satpathy⁷, Mark S. Anderson⁶, Terri M. Laufer⁸, Iannis Aifantis⁹,
8 Juliet M. Bartleson^{10,16}, Paul M. Allen¹⁰, Helena Paidassi¹¹, James M. Gardner^{6,12}, Marlon
9 Stoeckius^{5,17}, Dan R. Littman^{1,2†}

10

11
12 ¹ Molecular Pathogenesis Program, The Kimmel Center for Biology and Medicine of the
13 Skirball Institute, New York University School of Medicine, New York, NY, USA

14 ² Howard Hughes Medical Institute, New York, NY, USA

15 ³ Center for Genomics and Systems Biology, New York University, New York, NY, USA

16 ⁴ New York Genome Center, New York, NY, USA

17 ⁵ Technology Innovation Lab, New York Genome Center, New York, NY, USA

18 ⁶ Diabetes Center, University of California, San Francisco, San Francisco, CA, USA

19 ⁷ Department of Pathology, Stanford University, Stanford, CA 94305, USA. Parker Institute for
20 Cancer Immunotherapy, Stanford University, Stanford, CA 94305, USA, Gladstone-UCSF
21 Institute of Genomic Immunology, San Francisco, CA 94158, USA

22 ⁸ Department of Medicine, Perelman School of Medicine, University of Pennsylvania and
23 Department of Medicine, C. Michael Crescenz Veterans Administration Medical Center,
24 Philadelphia, PA, USA

25 ⁹ Department of Pathology, New York University School of Medicine, New York, NY, USA

26 ¹⁰ Department of Pathology and Immunology, Washington University School of Medicine, St.
27 Louis, MO, USA

28 ¹¹ CIRI, Centre International de Recherche en Infectiologie "Team Normal and Pathogenic B
29 cells" Univ Lyon Inserm U1111 Université Claude Bernard Lyon 1 CNRS UMR5308 ENS de
30 Lyon, F-69007 Lyon France.

31 ¹² Department of Surgery, University of California, San Francisco, San Francisco, CA, USA

32
33 Current addresses: ¹³Calico Life Sciences, LLC, South San Francisco, CA, USA; ¹⁴National
34 Institute for Biological Sciences, Beijing, China; ¹⁵Fred Hutchinson Cancer Center, Seattle, WA
35 USA; ¹⁶Buck Institute for Research on Aging, Novato, CA, USA; ¹⁷10X Genomics, Stockholm,
36 Sweden
37
38 [†] E-mail: dan.littman@med.nyu.edu

39 **Abstract**

40

41 The mutualistic relationship of gut-resident microbiota and cells of the host immune system
42 promotes homeostasis that ensures maintenance of the microbial community and of a poised, but
43 largely non-aggressive, immune cell compartment^{1,2}. Consequences of disturbing this balance,
44 by environmental or genetic factors, include proximal inflammatory conditions, like Crohn's
45 disease, and systemic illnesses, both metabolic and autoimmune. One of the means by which
46 this equilibrium is achieved is through induction of both effector and suppressor or regulatory arms
47 of the adaptive immune system. In mice, *Helicobacter* species induce regulatory (iTreg) and
48 follicular helper (Tfh) T cells in the colon-draining mesenteric lymph nodes under homeostatic
49 conditions, but can instead induce inflammatory Th17 cells when iTreg cells are compromised^{3,4}.
50 How *Helicobacter hepaticus* and other gut bacteria direct T cells to adopt distinct functions
51 remains poorly understood. Here, we investigated which cells and molecular components are
52 required to convey the microbial instruction for the iTreg differentiation program. We found that
53 antigen presentation by cells expressing ROR γ t, rather than by classical dendritic cells, was both
54 required and sufficient for iTreg induction. These ROR γ t⁺ cells, likely to be type 3 innate lymphoid
55 cells (ILC3) and/or a recently-described population of Aire⁺ cells termed Janus cells⁵, require the
56 MHC class II antigen presentation machinery, the chemokine receptor CCR7, and α_v integrin,
57 which activates TGF- β , for iTreg cell differentiation. In the absence of any of these, instead of
58 iTreg cells there was expansion of microbiota-specific pathogenic Th17 cells, which were induced
59 by other antigen presenting cells (APCs) that did not require CCR7. Thus, intestinal commensal
60 microbes and their products target multiple APCs with pre-determined features suited to directing
61 appropriate T cell differentiation programs, rather than a common APC that they endow with
62 appropriate functions. Our results illustrate the ability of microbiota to exploit specialized functions

63 of distinct innate immune system cells, targeting them to achieve the desired composition of
64 equipoised T cells, thus maintaining tolerance.

65

66 **Main**

67

68 A subset of bacterial species among the hundreds that comprise the gut microbiota elicit
69 stereotypic antigen-specific T cell differentiation programs through mechanisms yet to be
70 elucidated. It is generally accepted that conventional (or classical) dendritic cells (cDC) that
71 migrate from tissue to the inductive sites in lymph nodes present microbial antigens to activate
72 and promote differentiation of naive antigen-specific T cells^{4,6-10}. However, the antigen presenting
73 cells (APCs) that execute these functions according to instructions of distinct intestinal bacterial
74 species have not been clearly defined. We have chosen to study the APC requirements for T cell
75 responses to *H. hepaticus* (Hh), which elicits iTreg, Tfh, or pathogenic Th17 cells under different
76 conditions³.

77

78 **Selective requirement of APC subsets for gut microbiota-specific iTreg and inflammatory**
79 **Th17 cell differentiation**

80

81 To study the properties of antigen-presenting cells that direct the differentiation of microbiota-
82 specific iTreg cells, we transferred into Hh-colonized mice naive Hh-specific CD4⁺ T cells from
83 HH7-2 TCR transgenic mice³. CFSE-labeled transferred T cells exhibited robust proliferation by
84 day 3 in colon-draining C1 mesenteric lymph nodes (MLN) of wild type (WT) mice, with up-
85 regulation of Foxp3 and ROR γ t, characteristic of colonic iTreg cells^{11,12}. In contrast, in mice
86 deficient for antigen presentation by DC (and, potentially, other cells: *CD11c-Cre;I-Ab^{ff}*,
87 designated as *MHCII^{ΔCD11c}*), there was no expression of Foxp3 by the Hh-specific T cells, but,
88 surprisingly, there was substantial proliferation of these cells, with up-regulation of ROR γ t (Fig.

89 1a). At 2-3 weeks after transfer, there was expansion in the colonic lamina propria of ROR γ t- and
90 T-bet-expressing Hh-specific T cells in mutant mice, characteristic of a pro-inflammatory program
91 (Extended Data Fig. 1a-c). Endogenous T cells also displayed this phenotype, with fewer Foxp3 $^{+}$
92 ROR γ t $^{+}$ iTreg and expansion of Th17 cells (Extended Data Fig. 1b). This result suggested that
93 antigen presentation by *Cd11c*-lineage cells is required for iTreg cell differentiation, but that it is
94 dispensable for the differentiation of pro-inflammatory Th17 cells.

95
96 The chemokine receptor CCR7 mediates migration of DC and T cells into lymph nodes, where
97 adaptive immune responses are initiated, and is critical for tolerogenic responses to food
98 antigens¹³. In CCR7-deficient mice, iTreg induction in response to Hh colonization failed
99 (Extended Data Fig. 1d), in agreement with the recent demonstration of a CCR7 requirement for
100 the differentiation of iTreg cells specific for other *Helicobacter* species⁶. However, we observed
101 robust priming and proliferation of ROR γ t $^{+}$ Hh-specific T cells in CCR7-deficient mice (Extended
102 Data Fig. 1d). In *CD11c-Cre;Ccr7^{ff}* conditional mutant mice¹⁴ (designated *Ccr7^{ΔCD11c}*), transferred
103 Hh-specific T cells failed to differentiate into iTreg cells, despite exhibiting robust proliferation, as
104 in CCR7-deficient mice (Fig. 1b). In the colon of these mice, *Hh*-specific iTreg cells were rare, but
105 there was accumulation of inflammatory Th17 cells along with elongation of the crypts (Fig. 1c,
106 Extended Data Fig. 1e,f). Together, our results indicate that, unlike iTreg, microbiota-specific
107 inflammatory Th17 cell differentiation does not depend on either CCR7 or antigen presentation
108 by CD11c-expressing cells.

109
110 **Antigen presentation by *ROR γ t*-lineage cells is required for microbiota-induced iTreg cell
111 differentiation**

112

113 Classical DC, which have been broadly divided into cDC1 and cDC2, comprise multiple cell
114 subsets that differ in their ontogeny, location, and transcription factor dependency^{15,16}. Both cDC1
115 and cDC2 have been proposed to initiate iTreg responses, largely based on their ability to induce
116 Treg cell differentiation *in vitro*^{9,17}. However, *in vivo* depletion of cDC1 or cDC2 failed to
117 phenocopy iTreg loss (Extended Data Fig. 2a-c), in agreement with previous reports^{6,18-20}. These
118 findings suggested that antigen presentation by a rare uncharacterized *Cd11c*-lineage myeloid or
119 non-myeloid cell subset is required for iTreg cell differentiation. To identify putative antigen
120 presenting cell populations targeted by *CD11c-cre*, we performed CITE-seq analysis of cells
121 isolated from MLN of Hh-colonized *CD11c-Cre;ROSA26LSLtdTomato* (designated *tdTomato-*
122 *ON^{ΔCD11c}*) fate-map mice (Fig. 2a and Extended Data Fig. 3a,b). In addition to expected myeloid
123 cell subsets, we identified both ILC3 and a recently described *Aire⁺ ROR γ t⁺* population, named
124 Janus cells (JC)^{5,21}, among the *tdTomato⁺* cells, and these also expressed MHCII (Fig. 2b and
125 Extended Data Fig. 3b). Using a gating strategy for JC (Extended Data Fig. 4a-d), we confirmed
126 that they, like ILC3, express *Rorc* (Extended Data Fig. 3a). Consistent with this, *GFP⁺* ILC3 and
127 JC from the C1 MLN of *ROR γ t-eGFP* mice expressed both *CD11c* and *CD11b* or mostly *CD11c*,
128 respectively and were both targeted by *CD11c-Cre* (Fig. 2c, Extended Data Fig. 3b and 4e).
129 Accordingly, many fewer *ROR γ t⁺* cells from MLN of *MHCII^{ΔCD11c}* mice expressed MHCII, as
130 compared to WT littermates (Extended Data Fig. 5a).

131
132 Expression of MHCII by ILC3 was reported to prevent microbiota-dependent expansion of
133 inflammatory T cells in the intestine, and was proposed to mediate negative selection of those
134 cells²². Our results suggested that *CD11c-Cre*-expressing *ROR γ t⁺* cells may, instead, be required
135 for the differentiation of microbiota-specific iTreg cells. This was confirmed by examining iTreg
136 cell differentiation in mice whose MHCII was inactivated in presumptive ILC3 and JC (*ROR γ t-*
137 *Cre;I-AB^{II}*, designated as *MHCII^{ΔROR γ t}*). Despite expression of MHCII in cDC2 of these mutant

138 mice (Fig. 2d), there was complete loss of Hh-specific iTreg cell differentiation in colon-draining
139 MLN, but intact priming and subsequent expansion of pathogenic Th17 cells in the large intestine
140 lamina propria (Fig. 2e,f, Extended Data Fig. 5b). Both the donor Hh-specific and host T cells
141 exhibited loss of iTreg and increase in IFN γ - and IL-17A-producing CD4 $^{+}$ T cells in the large
142 intestine lamina propria (Fig. 2f, Extended Data Fig. 5c-e). Similar results were observed with Hh-
143 specific T cells in another conditional mutant strain, *ROR γ t-Cre; H2-DMa ff* mice (*H2-DMa $^{\Delta ROR\gamma t}$*)
144 deficient in H2-DMa, the mouse equivalent of HLA-DM, required for displacement of invariant
145 chain peptide and loading of processed peptide on MHCII molecules²³. This result confirms that
146 the antigen processing machinery is required in ROR γ t $^{+}$ APCs for induction of microbiota-specific
147 iTregs (Extended Data Fig. 5f).

148

149 **CCR7-dependent migration by ROR γ t-lineage cells is required for microbiota-induced**
150 **iTreg cell differentiation**

151

152 Intestinal ILC3 have been reported to also employ CCR7 for migration to draining MLN^{24,25}. We
153 found expression of *Ccr7* in both ILC3 and JC (Extended Data Fig. 3a and 6a). We therefore
154 asked whether CCR7 is required for migration of ROR γ t $^{+}$ APCs rather than classical DC for iTreg
155 induction. Indeed, Hh-specific iTreg cell differentiation was abrogated in the MLN of *Ccr7 $^{\Delta ROR\gamma t}$*
156 mice (Fig. 3a). In the colon of *Ccr7 $^{\Delta ROR\gamma t}$* mutant mice, there was skewing of Hh-specific T cells
157 towards a Th1-Th17 inflammatory program after 2-3 weeks of adoptive T cell transfer, although
158 this was less marked than in *Ccr7 $^{\Delta CD11c}$* mice, and elongation of crypts was not observed (Fig. 3b
159 and data not shown). To determine whether loss of CCR7 affects migration of ROR γ t $^{+}$ cells to the
160 MLN, we reconstituted irradiated mice with equal numbers of WT and *ROR γ t-Cre;Ccr7 ff*
161 (*Ccr7 $^{\Delta ROR\gamma t}$*) bone marrow cells. Although there was no effect on the ratio of WT and mutant
162 migratory DC, there was a substantial reduction in the proportion of CCR7-deficient lymphoid

163 tissue inducer (LTi)-like ILC3, but no significant difference in the proportions of other ROR γ t $^+$ cells
164 in the MLN (Fig 3c and Extended Data Fig. 6b-d). Similarly, in *Ccr7* $^{\Delta CD11c}$ mice, LTi-like ILC3 lost
165 CCR7 expression and were reduced in number in the MLN (Extended Data Fig. 6e,f). To further
166 study a potential role for JC, we examined the T cell response to Hh in *RORyt*-*cre*; *Aire* ff mice and
167 in Aire-DTR bone marrow-reconstituted mice treated with diphtheria toxin. In neither case was
168 there an effect on Hh-specific iTreg cell differentiation (Extended Data Fig. 7a,b). We cannot,
169 however, rule out a role for JC, as Aire may not be required for the microbiota-dependent iTreg
170 inductive function of these cells and residual cells in DT-treated animals may be sufficient to
171 support iTreg cell differentiation. Together, these results indicate that ROR γ t $^+$ APC, either LTi-like
172 ILC3 or JC, migrate to the MLN, where they present microbial antigen to naïve T cells to induce
173 iTreg cell differentiation, and that their failure to migrate results, instead, in inflammatory Th17 cell
174 differentiation.

175

176 **Integrin α_v expression by ROR γ t-lineage antigen presenting cells is required for iTreg
177 differentiation**

178

179 Differentiation of iTreg cells requires TGF- β signaling in CD4 $^+$ T cells, and defects in this pathway
180 result in spontaneous colitis^{3,11}. TGF- β is released from its latent form on cell surfaces or
181 extracellular matrix following physical interaction with integrins $\alpha_v\beta_6$ or $\alpha_v\beta_8$ ²⁶⁻²⁸. Loss of integrins
182 β_8 or α_v in hematopoietic cells, including in *CD11c*-*Cre*; *Itgb8* ff mice, resulted in reduced colonic
183 Tregs and in multiorgan inflammation²⁹⁻³¹. Consistent with those observations, differentiation of
184 adoptively transferred Hh-specific T cells into iTreg cells was abrogated both following treatment
185 of mice with anti- β_8 antibody and in *CD11c*-*Cre*; *Itgav* ff (*Itgav* $^{\Delta CD11c}$) recipient mice (Fig. 4a,b). We
186 examined iTreg cell differentiation in mice with conditional inactivation of *Itgav* in ROR γ t $^+$ APCs
187 and in T cells (*Itgav* $^{\Delta ROR\gamma t}$) (Fig. 4c,d). In the colon-draining MLN of *Itgav* $^{\Delta ROR\gamma t}$ mice, there was loss

188 of integrin α_v (CD51) expression on both ILC3 and JC, and adoptively transferred Hh-specific T
189 cells failed to express Foxp3 (Fig. 4c and Extended Data Fig. 8a). The MLN were increased in
190 size (Extended Data Fig. 8b) and the Hh-specific T cells expressed ROR γ t, but, unlike in control
191 littermates, they also had elevated T-bet, along with a substantial decrease in CCR6, consistent
192 with reduced TGF- β signaling (Extended Data Fig. 8c). Notably, β_8 antibody blockade resulted in
193 the same phenotype (Extended Data Fig. 8d). In the colonic lamina propria of *Itgav* ^{$\Delta ROR\gamma$ t} mice,
194 there was loss of both Hh-specific and host-derived iTreg cells, with skewing of CD4 $^+$ T cells
195 towards IFN γ $^+$ Th1 and pathogenic Th17 programs (Fig. 4d, Extended Data Fig. 8e), suggesting
196 that expression of integrin α_v on ROR γ t $^+$ APCs, likely in partnership with integrin β_8 , is a general
197 requirement for intestinal iTreg cell differentiation. Although ILC3 express higher levels of CD51
198 (Extended Data Fig. 8a), single-cell RNA sequencing analysis of GFP $^+$ cells from pooled lymph
199 nodes of *Aire* reporter mice³² showed clustering of JCs into three discrete subpopulations, with
200 JC2 and JC3 expressing high levels of *Itgav* and *Itgb8* (Extended Data Fig. 9a-e). JC and a fraction
201 of ILC3, obtained from *Itgb8-tdTomato* reporter mice³³, were found to express tdTomato
202 (Extended Data Fig. 9f), and we therefore cannot exclude the requirement of either cell type for
203 iTreg differentiation. Differentiation of iTreg cells was normal in *CD4-Cre;Itgav*^{ff} mice (Extended
204 Data Fig. 8f), consistent with a role of the integrin in ROR γ t $^+$ APCs rather than in TCR $\alpha\beta$ T cells.
205 Furthermore, we reconstituted mice after irradiation with a mix of MHCII ^{$\Delta CD11c$} and *Itgav* ^{$\Delta ROR\gamma$ t} bone
206 marrow cells, resulting in binary expression of MHCII or integrin α_v . In these mice, iTreg cell
207 differentiation was abolished, consistent with a requirement for both antigen presentation and
208 activation of TGF- β by the same APC, coupling T cell activation with differentiation cues (Fig. 4e-
209 f, Extended Data Fig. 8g).

210

211 **Antigen presentation by ROR γ t $^+$ APCs is sufficient to promote iTreg cell differentiation**

212

213 Our results support a role for *ROR γ t*⁺ APCs in microbiota-specific iTreg differentiation, but do not
214 rule out a requirement for additional conventional antigen presenting cells. Moreover, a population
215 of DC (T-bet-negative cDC2) was recently reported to express ROR γ t³⁴, raising the possibility that
216 neither ILC3 nor JC is relevant in iTreg cell differentiation. To examine a potential role for a rare
217 DC subset, we employed *zbtb46-Cre*, considered to specifically target cDC, and *zbtb46* reporter
218 mice. Because *zbtb46-Cre;Ccr7*^{fl/fl} mice (CCR7^{Δzbtb46}) were unable to support microbiota-
219 dependent iTreg cell differentiation (Extended Data Fig. 10a), we profiled by CITE-seq sorted
220 cells from C1 mLN of *zbtb46-eGFP; ROR γ t-Cre;ROSA26LSLtdTomato (tdTomato-ON*^{ROR γ t}*)* mice,
221 expressing one or both fluorescent reporters, gated to exclude B and T cells (Extended Data Fig.
222 10b). Surprisingly, GFP expression was identified on all ILC3 and fate-mapped JC. *Zbtb46*
223 expression on ILC3 was confirmed using *mKate2-ON*^{zbtb46}; *ROR γ t-eGFP* mice (Extended Data
224 Fig. 10c). We identified a few migratory cDC2 among tdTomato⁺ GFP⁺ cells in *zbtb46-eGFP;*
225 *tdTomato-ON*^{ROR γ t} mice, but these did not form a subcluster to suggest a unique gene signature
226 and did not exhibit active *Rorc* or integrin α_v mRNA and protein expression (Extended Data Fig.
227 10d-f), suggesting that they are unlikely to be ROR γ t⁺ APCs required to direct iTreg cell
228 differentiation. We performed three-dimensional intravital imaging studies to visualize interactions
229 of newly-primed Hh-specific T cells with DC and ROR γ t⁺ APCs populations in C1 MLN. We utilized
230 *mKate2-ON*^{zbtb46}; *ROR γ t-eGFP* mice to visualize cDC (mKate2⁺) and ROR γ t⁺ APCs (eGFP⁺ and
231 mKate2). However, given that the efficiency of *zbtb46-Cre*-mediated activation of the mKate2
232 reporter was low (~20% for *ROR γ t*⁺ APCs and cDC populations) (Extended Data Fig. 11a), we
233 additionally utilized cell morphology and size analysis to distinguish the few host-derived GFP⁺ T
234 cells from GFP⁺ ROR γ t⁺ APCs. We next transferred dye-labeled *Nur77-eGFP* Hh-specific T cells
235 into these fluorescent reporter host mice to measure direct interactions of primed T cells (which
236 up-regulate *Nur77*) with DC and ROR γ t⁺ APCs at 15 h after adoptive transfer. Approximately 81%

237 of GFP⁺ primed Hh-specific T cells were found in contact with at least one *RORγt*⁺ APC
238 with/without DC, as opposed to only ~31% of the non-primed T cells (Extended Data Fig. 11b,c).

239
240 Our imaging study and results with conditional mutant mice did not rule out a contribution by DC
241 towards Hh-specific T cell activation and iTreg differentiation. We therefore wished to determine
242 whether antigen presentation limited to only *RORγt*-Cre-expressing cells was sufficient to allow
243 for iTreg cell differentiation. For this purpose, we used mice that express MHCII only in *RORγt*⁺
244 APCs, and not in DC or other APCs (*RORγt*-Cre; *I-AB*^{-/sl}, designated *MHCII-ON*^{*RORγt*}). We
245 reconstituted irradiated congenic mice with bone marrow from *MHCII*^{*ΔCD11c*} mice with or without
246 bone marrow from WT or *MHCII-ON*^{*RORγt*} mice (Fig. 5a). Flow cytometry analysis confirmed MHCII
247 expression by *RORγt*⁺ cells, but not DC from the C1 MLN and the colon lamina propria of
248 *MHCII*^{*ΔCD11c*}; *MHCII-ON*^{*RORγt*} bone marrow-reconstituted mice (Fig. 5b, Extended Data Fig.
249 12a). As expected, in control mice reconstituted with only *MHCII*^{*ΔCD11c*} bone marrow cells,
250 in which no MHCII expression was detected in either *RORγt*⁺ APC or DC, there was no
251 differentiation of adoptively transferred Hh-specific iTreg cells, but there was, instead,
252 differentiation of *RORγt*⁺*Tbet*⁺ inflammatory Th17 cells (Fig. 5c,d). In contrast, antigen
253 presentation by *RORγt*⁺ cells alone was sufficient to rescue iTreg cell differentiation and
254 suppression of inflammatory T cells in response to Hh colonization, as seen in mice reconstituted
255 with *MHCII*^{*ΔCD11c*} plus *MHCII-ON*^{*RORγt*} bone marrow cells (Fig. 5c,d), or with only *MHCII-ON*^{*RORγt*}
256 cells (Extended Data Fig. 12c). There was similar rescue of endogenous iTreg cell differentiation
257 in mice having the gain-of-function MHCII in *RORγt*⁺ cells (Extended Data Fig. 12b). It should be
258 noted that whereas there was rescue of Hh-directed iTreg cell differentiation in mice reconstituted
259 with *MHCII-ON*^{*RORγt*} bone marrow, there was a marked absence of Bcl6-expressing Tfh cells,
260 which are also induced by Hh (Fig. 5c,d; Extended Data Fig. 12c). Interestingly, Tfh cells were
261 present in mice reconstituted with only *MHCII-ON*^{*CD11c*} bone marrow, suggesting that their

262 differentiation requires antigen presentation by DC and/or B cells, as proposed previously³⁵
263 (Extended Data Fig. 12c). We conclude that *ROR γ t⁺* APC, ILC3 and/or JC, are specialized to
264 prime naive microbiota-specific T cells and guide their differentiation into iTregs, but other APCs
265 are required to guide the differentiation of microbiota-specific pathogenic Th17 cells and Tfh cells.

266

267 **Discussion**

268

269 The composition of the intestinal microbiota influences host immune functions that contribute to
270 anti-microbial host defense, inflammatory disease, and anti-tumor immunity. Transmission of
271 information from gut microbes to immune system cells remains poorly understood. The current
272 results indicate that *ROR γ t⁺* cells, either JC, whose transcriptional profile suggests a role in
273 promoting immunological tolerance⁵, or type 3 innate lymphoid cells previously implicated in
274 restraining microbiota-dependent Th1/Th17 inflammatory responses in the gut^{36,37}, do so in large
275 part by conveying signals from the microbiota to naive bacteria-specific T cells, activating them
276 and guiding their differentiation towards a unique iTreg cell program. *ROR γ t⁺* cells defective for
277 CCR7-mediated migration (either to or within the MLN), MHCII antigen presentation, or av β 8
278 function (presumably through activation of TGF- β), failed to induce the iTreg program. Intriguingly,
279 under such circumstances there was expansion of pathogenic Th17 cells that promoted intestinal
280 inflammation. We previously demonstrated that a T cell-intrinsic c-Maf deficiency prevented iTreg
281 cell differentiation, and similarly allowed for microbiota-dependent differentiation of pathogenic
282 Th17 cells³. Together, these findings suggest that iTreg cells restrain the priming, proliferation,
283 and differentiation of Th17 cells in the MLN. The APC(s) that directs pathogenic Th17 cell
284 differentiation does not require CCR7, and it is not targeted in CD11c-Cre mice, and is, therefore,
285 most likely not a cDC, but its identity is currently not known. One hypothesis is that iTreg cells
286 might not only inhibit Th17 cell differentiation and function but also may inhibit the function of the

287 CCR7-independent Th17 inducer APC (Extended Data Fig. 13).

288

289 It has been proposed that intrinsically different APC subsets direct distinct T cell responses³⁸, but
290 such processes have been difficult to demonstrate in the setting of immune responses *in vivo*.
291 Our study shows that a unique ROR γ t⁺ cell type instructs naïve microbiota-specific CD4⁺ T cells
292 to become iTreg cells, but does not support the differentiation of other T cell programs, including
293 Tfh cells, that are normally also induced by Hh intestinal colonization. Although our results are
294 most compatible with the ROR γ t⁺ APC being an ILC3 or Aire⁺ JC subset, we cannot rule out that
295 it may represent a novel ROR γ t⁺ cell type that cannot yet be categorized as either lymphoid or
296 DC-like. Definitive identification and characterization of this cell awaits more specific genetic tools
297 than those currently available. Nevertheless, our results clearly demonstrate the existence of
298 multiple APCs that are targeted by a specific commensal microbe to instruct diverse effector T
299 cell functions (Extended Data Fig. 13). The APCs may act hierarchically, as exemplified here by
300 ROR γ t⁺ cells that supersede the function of Th17-inducing APC. The existence and identity of
301 distinct cellular circuits responsible for the induction of iTregs and other T cell functional subsets
302 offers the opportunity to investigate the corresponding cells in humans and, potentially, to
303 modulate them therapeutically.

304

305 **Acknowledgements**

306

307 We thank members of the Littman lab, Juan J. Lafaille, and Susan Schwab for valuable discussion
308 and critical reading of the manuscript and Gabriela Romero-Meza for assistance with
309 experiments. We thank Dean Sheppard for advice and providing ADWA11 blocking Ab, S.Y. Kim
310 and the NYU Rodent Genetic Engineering Laboratory (RGEL) for rederivation of mutant mice,
311 and Cindy Loomis and the Experimental Pathology Research Laboratory of NYULMC for histology

312 of intestine samples. The Microscopy Core and the Genome Technology Core are partially
313 supported by NYU Cancer Center Support Grant NIH/NCI P30CA016087 at the Laura and Isaac
314 Perlmutter Cancer Center, S10 RR023704-01A1 and NIH S10 ODO019974-01A1. The
315 Experimental Pathology Research Laboratory is supported by National Institutes of Health Shared
316 Instrumentation grants S10OD010584-01A1 and S10OD018338-01. Caleb A. Lareau, Ansuman
317 T. Satpathy and James M. Gardner are recipients of the IGVF award UM1HG012076. This work
318 was supported by an Irvington Institute fellowship from the Cancer Research Institute (R.K.) and
319 a Jane Coffin Childs Fund fellowship (K.R.M.), the Helen and Martin Kimmel Center for Biology
320 and Medicine (D.R.L.); National Institutes of Health grants R01AI139540 (P.M.A.) and
321 R01AI158687 (D.R.L.), and the Howard Hughes Medical Institute (D.R.L.).

322

323 **Author Contributions**

324

325 R.K., T.N., K.R.M. and D.R.L. designed the study and analyzed the data; R.K. and T.N. performed
326 mouse genetic experiments with assistance from A.G; M.P., M.X., and J.T. performed early
327 experiments to launch the study. Intravital multiphoton microscopy (K.R.M. and R.K.), CITE-seq
328 studies (R.K, S.H. and M.S.), scRNA-seq (A.T.S., C.A.L), bioinformatics analyses (R.K, L.K., Y.H.,
329 J.G.). J.W., M.S.A., and J.M.G. provided biological samples, genomics data, and experimental
330 support. H.P., T.M.L., I.A., J.M.B., and P.M.A. contributed mouse strains and phenotypic analysis
331 (H.P.). R.K. and D.R.L. wrote the manuscript, with input from the other authors. D.R.L.
332 supervised the research.

333

334

335 **References**

336

337 1 Hooper, L. V., Littman, D. R. & Macpherson, A. J. Interactions between the microbiota
338 and the immune system. *Science* **336**, 1268-1273, doi:10.1126/science.1223490 (2012).

339 2 Ansaldo, E., Farley, T. K. & Belkaid, Y. Control of Immunity by the Microbiota. *Annu Rev
340 Immunol* **39**, 449-479, doi:10.1146/annurev-immunol-093019-112348 (2021).

341 3 Xu, M. *et al.* c-MAF-dependent regulatory T cells mediate immunological tolerance to a
342 gut pathobiont. *Nature* **554**, 373-377, doi:10.1038/nature25500 (2018).

343 4 Chai, J. N. *et al.* Helicobacter species are potent drivers of colonic T cell responses in
344 homeostasis and inflammation. *Science immunology* **2**, doi:10.1126/sciimmunol.aal5068
345 (2017).

346 5 Wang, J., Lareau, C.A., Bautista, J.L., Gupta, A.R., Sandor, K., Germino, J., Yin, Y.,
347 Arvedson, M.P., Reeder, G.C., Cramer, N.T., Xie, F., Ntranos, V., Satpathy, A.T., Anderson,
348 M.S., Gardner, J.M. Single-cell multiomics defines tolerogenic extrathymic Aire-
349 expressing populations with unique homology to thymic epithelium. *Sci. Immunol.* **6**
350 (2021).

351 6 Russler-Germain, E. V. *et al.* Gut Helicobacter presentation by multiple dendritic cell
352 subsets enables context-specific regulatory T cell generation. *eLife* **10**,
353 doi:10.7554/eLife.54792 (2021).

354 7 Darrasse-Jèze, G. *et al.* Feedback control of regulatory T cell homeostasis by dendritic
355 cells in vivo. *The Journal of experimental medicine* **206**, 1853-1862,
356 doi:10.1084/jem.20090746 (2009).

357 8 Durai, V. & Murphy, K. M. Functions of Murine Dendritic Cells. *Immunity* **45**, 719-736,
358 doi:10.1016/j.jimmuni.2016.10.010 (2016).

359 9 Esterházy, D. *et al.* Classical dendritic cells are required for dietary antigen-mediated
360 induction of peripheral T(reg) cells and tolerance. *Nature immunology* **17**, 545-555,
361 doi:10.1038/ni.3408 (2016).

362 10 Nussenzweig, M. C., Steinman, R. M., Gutchinov, B. & Cohn, Z. A. Dendritic cells are
363 accessory cells for the development of anti-trinitrophenyl cytotoxic T lymphocytes. *The*
364 *Journal of experimental medicine* **152**, 1070-1084, doi:10.1084/jem.152.4.1070 (1980).

365 11 Nutsch, K. *et al.* Rapid and Efficient Generation of Regulatory T Cells to Commensal
366 Antigens in the Periphery. *Cell Rep* **17**, 206-220, doi:10.1016/j.celrep.2016.08.092
367 (2016).

368 12 Esterhazy, D. *et al.* Compartmentalized gut lymph node drainage dictates adaptive
369 immune responses. *Nature* **569**, 126-130, doi:10.1038/s41586-019-1125-3 (2019).

370 13 Worbs, T. *et al.* Oral tolerance originates in the intestinal immune system and relies on
371 antigen carriage by dendritic cells. *The Journal of experimental medicine* **203**, 519-527,
372 doi:10.1084/jem.20052016 (2006).

373 14 Koscsó, B. *et al.* Gut-resident CX3CR1(hi) macrophages induce tertiary lymphoid
374 structures and IgA response in situ. *Science immunology* **5**,
375 doi:10.1126/sciimmunol.aax0062 (2020).

376 15 Mildner, A. & Jung, S. Development and function of dendritic cell subsets. *Immunity* **40**,
377 642-656, doi:10.1016/j.jimmuni.2014.04.016 (2014).

378 16 Anderson, D. A., 3rd, Dutertre, C. A., Ginhoux, F. & Murphy, K. M. Genetic models of
379 human and mouse dendritic cell development and function. *Nat Rev Immunol* **21**, 101-
380 115, doi:10.1038/s41577-020-00413-x (2021).

381 17 Coombes, J. L. *et al.* A functionally specialized population of mucosal CD103+ DCs
382 induces Foxp3+ regulatory T cells via a TGF-beta and retinoic acid-dependent
383 mechanism. *The Journal of experimental medicine* **204**, 1757-1764,
384 doi:10.1084/jem.20070590 (2007).

385 18 Persson, E. K. *et al.* IRF4 transcription-factor-dependent CD103(+)CD11b(+) dendritic
386 cells drive mucosal T helper 17 cell differentiation. *Immunity* **38**, 958-969,
387 doi:10.1016/j.jimmuni.2013.03.009 (2013).

388 19 Pool, L., Rivollier, A. & Agace, W. W. Deletion of IRF4 in Dendritic Cells Leads to Delayed
389 Onset of T Cell-Dependent Colitis. *J Immunol* **204**, 1047-1055,
390 doi:10.4049/jimmunol.1900775 (2020).

391 20 Wohn, C. *et al.* Absence of MHC class II on cDC1 dendritic cells triggers fatal
392 autoimmunity to a cross-presented self-antigen. *Science immunology* **5**,
393 doi:10.1126/sciimmunol.aba1896 (2020).

394 21 Yamano, T. *et al.* Aire-expressing ILC3-like cells in the lymph node display potent APC
395 features. *The Journal of experimental medicine* **216**, 1027-1037,
396 doi:10.1084/jem.20181430 (2019).

397 22 Hepworth, M. R. *et al.* Immune tolerance. Group 3 innate lymphoid cells mediate
398 intestinal selection of commensal bacteria-specific CD4(+) T cells. *Science* **348**, 1031-
399 1035, doi:10.1126/science.aaa4812 (2015).

400 23 Bartleson, J. M. *et al.* Strength of tonic T cell receptor signaling instructs T follicular
401 helper cell-fate decisions. *Nature immunology* **21**, 1384-1396, doi:10.1038/s41590-020-
402 0781-7 (2020).

403 24 Mackley, E. C. *et al.* CCR7-dependent trafficking of RORgamma(+) ILCs creates a unique
404 microenvironment within mucosal draining lymph nodes. *Nat Commun* **6**, 5862,
405 doi:10.1038/ncomms6862 (2015).

406 25 Kim, M. H., Taparowsky, E. J. & Kim, C. H. Retinoic Acid Differentially Regulates the
407 Migration of Innate Lymphoid Cell Subsets to the Gut. *Immunity* **43**, 107-119,
408 doi:10.1016/j.jimmuni.2015.06.009 (2015).

409 26 Wang, R. *et al.* GARP regulates the bioavailability and activation of TGFbeta. *Mol Biol*
410 *Cell* **23**, 1129-1139, doi:10.1091/mbc.E11-12-1018 (2012).

411 27 Lienart, S. *et al.* Structural basis of latent TGF-beta1 presentation and activation by
412 GARP on human regulatory T cells. *Science* **362**, 952-956, doi:10.1126/science.aau2909
413 (2018).

414 28 Qin, Y. *et al.* A Milieu Molecule for TGF-beta Required for Microglia Function in the
415 Nervous System. *Cell* **174**, 156-171 e116, doi:10.1016/j.cell.2018.05.027 (2018).

416 29 Lacy-Hulbert, A. *et al.* Ulcerative colitis and autoimmunity induced by loss of myeloid
417 alphav integrins. *Proc Natl Acad Sci U S A* **104**, 15823-15828,
418 doi:10.1073/pnas.0707421104 (2007).

419 30 Paidassi, H. *et al.* Preferential expression of integrin alphavbeta8 promotes generation
420 of regulatory T cells by mouse CD103+ dendritic cells. *Gastroenterology* **141**, 1813-1820,
421 doi:10.1053/j.gastro.2011.06.076 (2011).

422 31 Travis, M. A. *et al.* Loss of integrin alpha(v)beta8 on dendritic cells causes autoimmunity
423 and colitis in mice. *Nature* **449**, 361-365, doi:10.1038/nature06110 (2007).

424 32 Gardner, J. M. *et al.* Deletional tolerance mediated by extrathymic Aire-expressing cells.
425 *Science* **321**, 843-847, doi:10.1126/science.1159407 (2008).

426 33 Nakawesi, J. *et al.* alphavbeta8 integrin-expression by BATF3-dependent dendritic cells
427 facilitates early IgA responses to Rotavirus. *Mucosal Immunol* **14**, 53-67,
428 doi:10.1038/s41385-020-0276-8 (2021).

429 34 Brown, C. C. *et al.* Transcriptional Basis of Mouse and Human Dendritic Cell
430 Heterogeneity. *Cell* **179**, 846-863 e824, doi:10.1016/j.cell.2019.09.035 (2019).

431 35 Barnett, L. G. *et al.* B cell antigen presentation in the initiation of follicular helper T cell
432 and germinal center differentiation. *J Immunol* **192**, 3607-3617,
433 doi:10.4049/jimmunol.1301284 (2014).

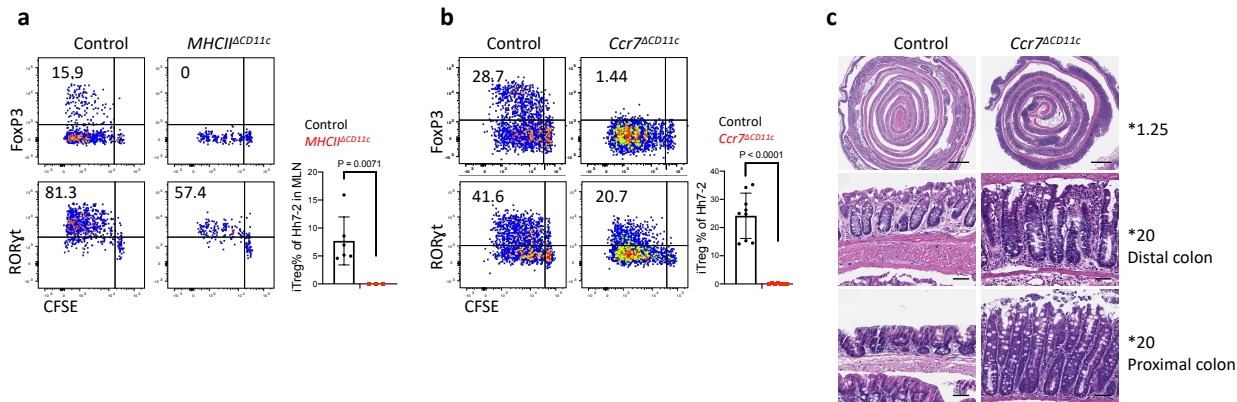
434 36 Hepworth, M. R. *et al.* Innate lymphoid cells regulate CD4+ T-cell responses to intestinal
435 commensal bacteria. *Nature* **498**, 113-117, doi:10.1038/nature12240 (2013).

436 37 Goto, Y. *et al.* Segmented filamentous bacteria antigens presented by intestinal
437 dendritic cells drive mucosal Th17 cell differentiation. *Immunity* **40**, 594-607,
438 doi:10.1016/j.jimmuni.2014.03.005 (2014).

439 38 Yin, X., Chen, S. & Eisenbarth, S. C. Dendritic Cell Regulation of T Helper Cells. *Annu Rev
440 Immunol* **39**, 759-790, doi:10.1146/annurev-immunol-101819-025146 (2021).

441

442

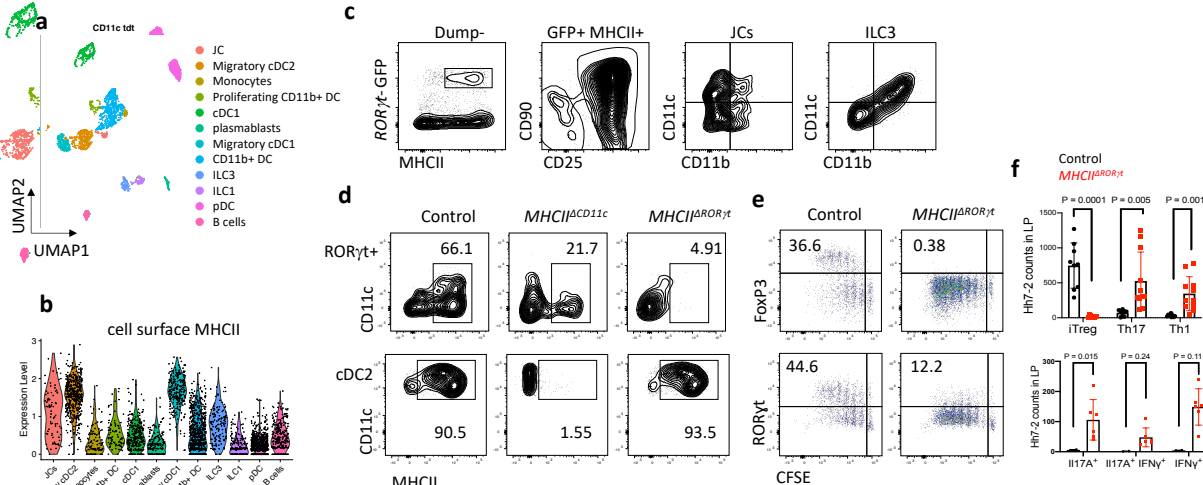


443

444

445 **Figure 1. Distinct requirements for antigen presentation and CCR7 expression in**
446 **differentiation of iTreg versus pathogenic Th17 cells.**

447 **a-b,** Hh-specific T cell proliferation and differentiation in Hh-colonized *CD11c-Cre;I-Ab*^{ff}
448 (*MHCII*^{ΔCD11c}) (n=3) and *I-Ab*^{ff} or *CD11c-Cre;I-Ab*^{f/f} littermate control mice (n=6) (a) and in
449 *Ccr7*^{ΔCD11c} (n = 7) and littermate control mice (n = 9) (b). CFSE-labeled naïve TCR transgenic
450 Hh7-2 T cells from the C1 MLN were assessed for cell proliferation and expression of FoxP3
451 and ROR γ t at 3 days after adoptive transfer. Representative flow cytometry (left) and aggregate
452 results (right). Data summarize two (a) and three (b) independent experiments. **c,**
453 Representative H&E histology in large intestine of mice with indicated genotypes. Scale bars
454 are 1 mm and 50 μ m, for 1.25X and 20X. respectively. All statistics were calculated by unpaired
455 two-sided Welch's t-test. Error bars denote mean \pm s.d. *p*-values are indicated in the figure.



456

457

458 **Figure 2. Antigen presentation by ROR γ t⁺ cells is required for microbiota-induced iTreg cell differentiation.**

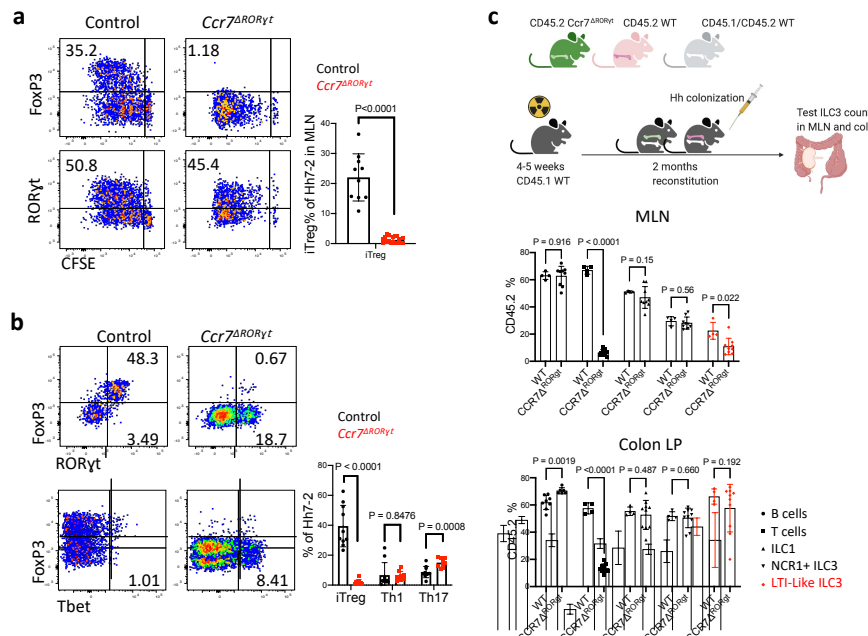
460 **a-b**, UMAP visualization of the *tdTomato-ON*^{CD11c} fate-map cell CITE-seq dataset, analyzed by
461 the WNN method (a), and Violin plot showing MHCII protein levels in the different cell clusters
462 (b). MLN cells from Hh-colonized *tdTomato-ON*^{CD11c} fate-map mice were gated for TCR β^- ,
463 TCR $\gamma\delta^-$, B220 $^-$, and *tdTomato* $^+$ cells were sorted for CITE-seq analysis. Cells were sorted from
464 two mice and labeled by hashing antibodies (n=2). **c**, CD11c and CD11b staining of ILC3 and
465 JC from MLN of Hh-colonized *ROR γ t-eGFP* mice, gated as indicated. **d**, MHCII expression in
466 ROR γ t⁺ cells (top) and DCs (bottom) from the MLN of Hh-colonized mice of the indicated
467 genotypes. ROR γ t⁺ cells were gated as TCR β^- , TCR $\gamma\delta^-$, B220 $^-$, ROR γ t⁺; DC were gated as
468 TCR β^- , TCR $\gamma\delta^-$, B220 $^-$, CD90 $^-$, CD11c $^+$, CD11b $^+$ SIRP α^+ . **e**, Hh7-2 cell proliferation and
469 differentiation in $MHCII^{ΔROR\gamma t}$ (n = 6) and *I-Ab*^{ff} littermate control mice (n = 6) at 3 days after
470 adoptive transfer into Hh-colonized mice. **f**, Hh7-2 T cell differentiation profiles (upper) and
471 cytokine production (lower) in the large intestine lamina propria at 22 days after transfer into
472 $MHCII^{ΔROR\gamma t}$ (n=11) and littermate controls (n=9). Differentiation was assessed by expression of

473 Foxp3, ROR γ t with or without T-bet, and T-bet. Data summarize two independent experiments.

474 All statistics were calculated by unpaired two-sided Welch's t-test. Error bars denote mean \pm s.d.

475 *p*-values are indicated on the figure.

476



477

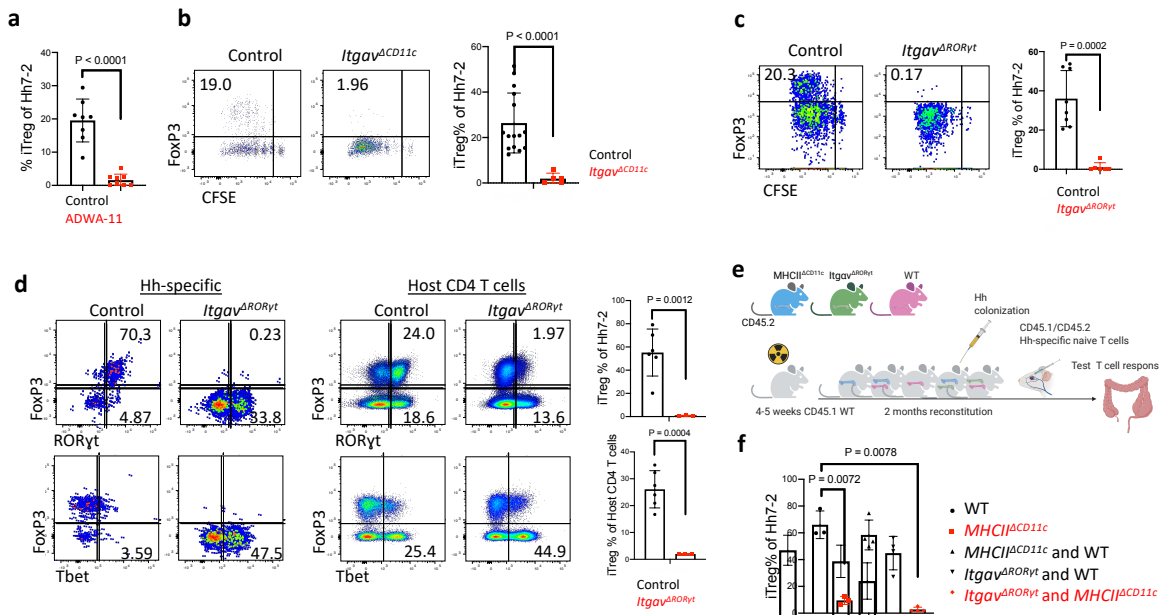
478

479 **Figure 3. ROR γ t⁺ cells require CCR7 to promote iTreg cell differentiation. a-b,**
480 Representative flow cytometry profiles (left) and aggregate data (right) for Hh7-2 T cell
481 proliferation and differentiation in MLN at 3 days (a) and their phenotype in large intestine at 14
482 days (b) following adoptive transfer into *Ccr7*^{ΔROR γ t} and littermate control mice. MLN: Control
483 mice n=10, *Ccr7*^{ΔROR γ t} mice n=20; LI: Control mice n=10, *Ccr7*^{ΔROR γ t} mice n=9. Data summarize
484 three independent experiments. Statistics were calculated by unpaired two-sided Welch's t-test.
485 **c**, Analysis of CCR7 requirement for ROR γ t⁺ cell accumulation in the MLN. Irradiated CD45.1
486 mice were reconstituted with equal number of bone marrow cells from CD45.2 *Ccr7*^{ΔROR γ t} and
487 CD45.1/CD45.2 WT mice or with CD45.2 WT and CD45.1/CD45.2 WT mice as controls.
488 Scheme is shown at the top (created with BioRender.com). Aggregate data shows the
489 frequency in MLN and colon lamina propria of CD45.2 WT (n=4) or CD45.2 *Ccr7*^{ΔROR γ t} (n=9)
490 cells within each subset, as indicated. Data summarize three independent experiments. All

491 statistics were calculated by unpaired two-sided Welch's t-test. Error bars denote mean \pm s.d. *p*-

492 values are indicated in the figure.

493



494

495

496 **Figure 4. Role of integrin $\alpha_v\beta_8$ in $ROR\gamma^t$ ⁺ antigen presenting cell-dependent iTreg cell**
497 **differentiation. a**, Frequency of iTreg cells among proliferating donor-derived Hh-specific cells
498 in the MLN at 3 days after transfer of naïve CFSE-labeled Hh7-2 T cells into mice treated with
499 200 μ g of ADWA11 blocking antibody (n=8) or left untreated (n=8), on the day of adoptive
500 transfer. Data summarize three independent experiments. **b**, Hh7-2 T cell proliferation and
501 differentiation in the MLN of *Itgav*^{ΔCD11c} (n=5) and littermate controls (n=15) at 3 days after
502 adoptive transfer. Data summarize three independent experiments. **c**, Proliferation and
503 differentiation of Hh-specific iTreg cells in the MLN of *Itgav*^{ΔROR γ t} (n=6) and littermate control
504 mice (n=8). CFSE-labeled Hh7-2 T cells were analyzed at 3 days following their adoptive
505 transfer into Hh-colonized mice. Representative flow cytometry profiles (left) and aggregate data
506 (right). Data summarize three independent experiments. **d**, Transcription factor expression in
507 Hh7-2 T cells (left panels) and in endogenous CD4 $^+$ T cells (right panels) from colon lamina
508 propria (LP) at 10 days after adoptive transfer into *Itgav*^{ΔROR γ t} mice (n=3) and control littermates

509 (n=6). Data summarize two independent experiments. Representative dot plots and aggregate
510 data are shown (right panels). **e**, Scheme for mixed bone marrow chimeric mouse experiment,
511 with control, *Itgav*^{ΔROR_{yt}} or *MHCII*^{ΔCD11c} cells administered to irradiated host mice (created with
512 BioRender.com). **f**, Bar graphs showing iTreg frequency among Hh7-2 T cells in the colon LP at
513 10 days after their transfer into the bone marrow chimeric mice, reconstituted with different
514 combinations of donor cells as indicated. Control mice (n=3), *MHCII*^{ΔCD11c} (n=3), *MHCII*^{ΔCD11c}
515 and WT (n=4), *Itgav*^{ΔROR_{yt}} and WT (n=4) and *MHCII*^{ΔCD11c} and *Itgav*^{ΔROR_{yt}} (n=4). All statistics
516 were calculated by unpaired two-sided Welch's t-test. Error bars denote mean ± s.d. *p*-values
517 are indicated in the figure.

518

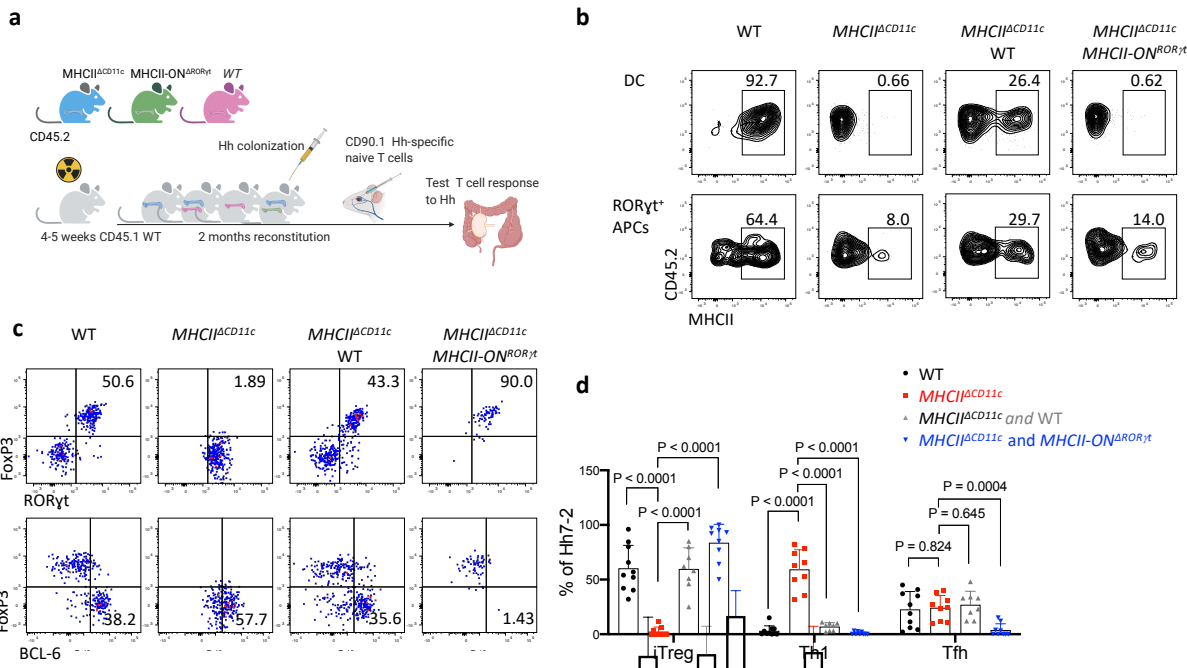
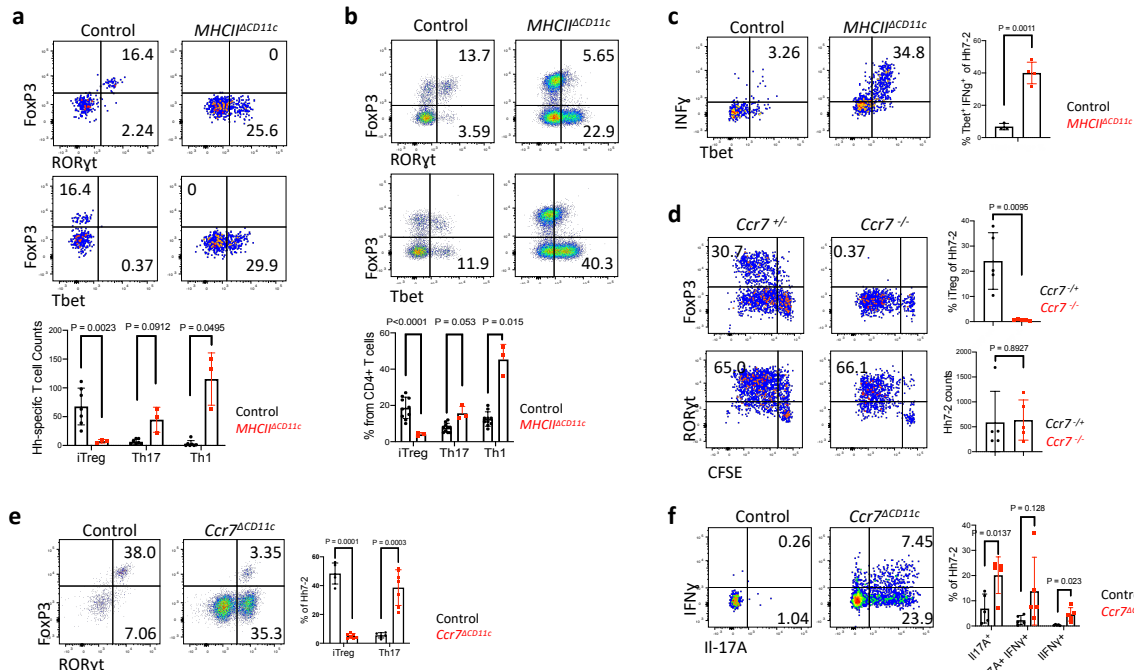
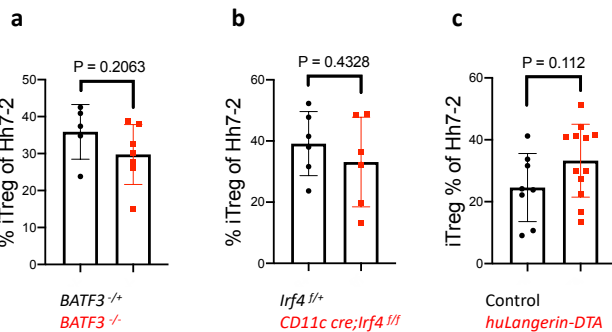


Figure 5. Antigen presentation by ROR γ t $^+$ cells is sufficient to promote iTreg cell differentiation. a, Experimental design (created with BioRender.com). b, MHCII frequency in donor bone marrow-derived cDC2 (gated TCR β $^-$, TCR $\gamma\delta$ $^-$, B220 $^-$, CD45.2 $^+$, CD11c $^+$, CD11b $^+$ Sirpa $^+$) and ROR γ t $^+$ cells (gated as TCR β $^-$, TCR $\gamma\delta$ $^-$, B220 $^-$, ROR γ t $^+$, CD45.2 $^+$) in MLN from chimeric mice reconstituted with combinations of donor BM cells as indicated. c, Representative flow cytometry of Hh7-2 T cell differentiation in colon lamina propria of Hh-colonized bone marrow chimeric mice, 12 days after transfer of naive TCR transgenic T cells. d, Aggregate data for differentiation of Hh7-2 T cells in bone marrow chimeric mice reconstituted with cells of indicated genotypes. WT (n=10), MHCII $^{\Delta CD11c}$ (n=9), MHCII $^{\Delta CD11c}$ and WT (n=8), MHCII $^{\Delta CD11c}$ and MHCII-ON $^{\Delta ROR\gamma t}$ (n=9). Data summarize three independent experiments. All statistics were calculated by unpaired two-sided Welch's t-test. Error bars denote mean \pm s.d. p-values are indicated in the figure.



534

535 **Extended Data Fig. 1. Cells targeted by CD11c-Cre and consequences for Hh-specific T**
 536 **cell differentiation. a, Phenotype of Hh7-2 TCR transgenic T cells in the colon lamina propria**
 537 **at 10 days after transfer into Hh-colonized $MHCII^{\Delta CD11c}$ (n=3) and control mice (n=7), as**
 538 **indicated. b, Phenotype of host CD4 $^+$ T cells from mice in (a); $MHCII^{\Delta CD11c}$ (n=3) and control**
 539 **mice (n=10), as indicated. c, Cytokine profile of Hh7-2 T cells shown in (a); $MHCII^{\Delta CD11c}$ (n=4)**
 540 **and control mice (n=3). d, Proliferation and differentiation of Hh-specific iTreg and Th17 cells in**
 541 **the MLN of $Ccr7^{-/-}$ (n=5) and littermate control mice (n=5). CFSE-labeled Hh7-2 T cells were**
 542 **analyzed at 3 days following their adoptive transfer into Hh-colonized mice. Data summarize two**
 543 **independent experiments. e-f, Transcription factor (e) and intracellular cytokine (f) profiles of**
 544 **Hh7-2 T cells in the large intestine of $Ccr7^{\Delta CD11c}$ (n=7 or 5, for transcription factors and**
 545 **cytokines, respectively) and littermate control (n=5) mice, at 10 days after adoptive transfer.**
 546 **Data summarize two independent experiments. Representative flow panels and aggregate data**
 547 **are shown for each analysis. All statistics were calculated by unpaired two-sided Welch's t-test.**
 548 **Error bars denote mean \pm s.d. p-values are indicated in the figure.**



549

550 **Extended Data Fig. 2. cDC1 or cDC2 are not required for iTreg differentiation. a-c,**

551 Proportion in MLN of Hh7-2 with the iTreg phenotype at 3 days after transfer into *BATF3*^{-/-} (a)

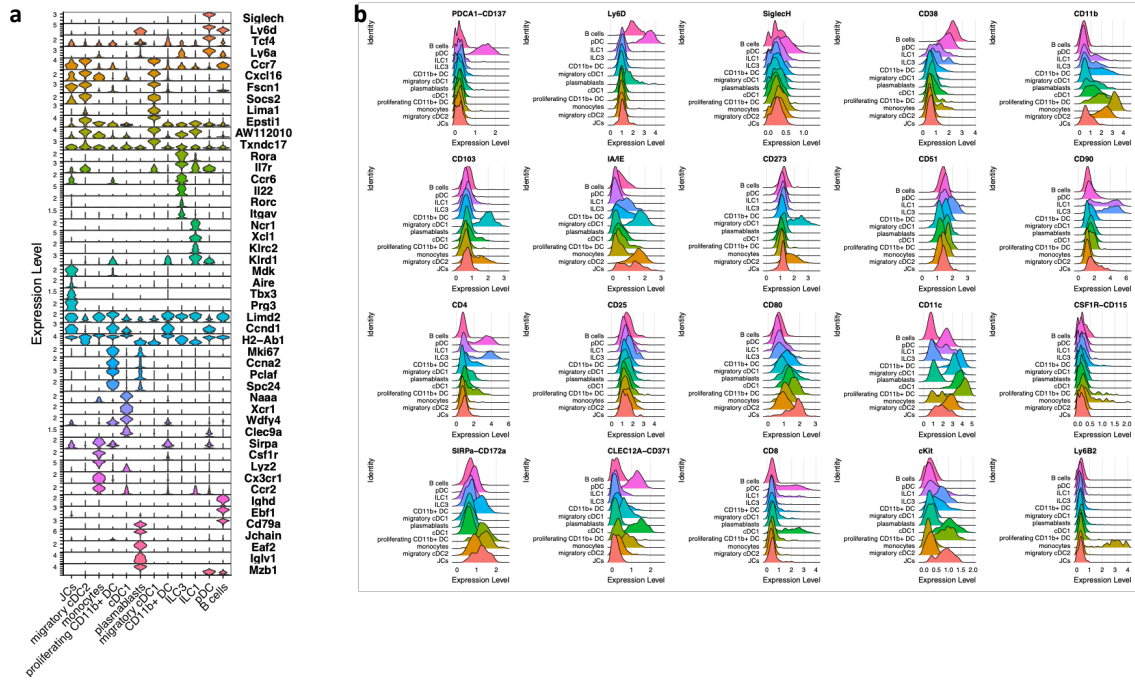
552 ($n=7$), *IRF4*^{CD11c} (b) ($n=6$), and *huLangerin* (*CD207*)-DTA (c) ($n=12$) mice (red) and indicated

553 littermate controls (black). Data summarize at least two independent experiments. All statistics

554 were calculated by unpaired two-sided Welch's t-test. Error bars denote mean \pm s.d. *p*-values

555 are indicated in the figure.

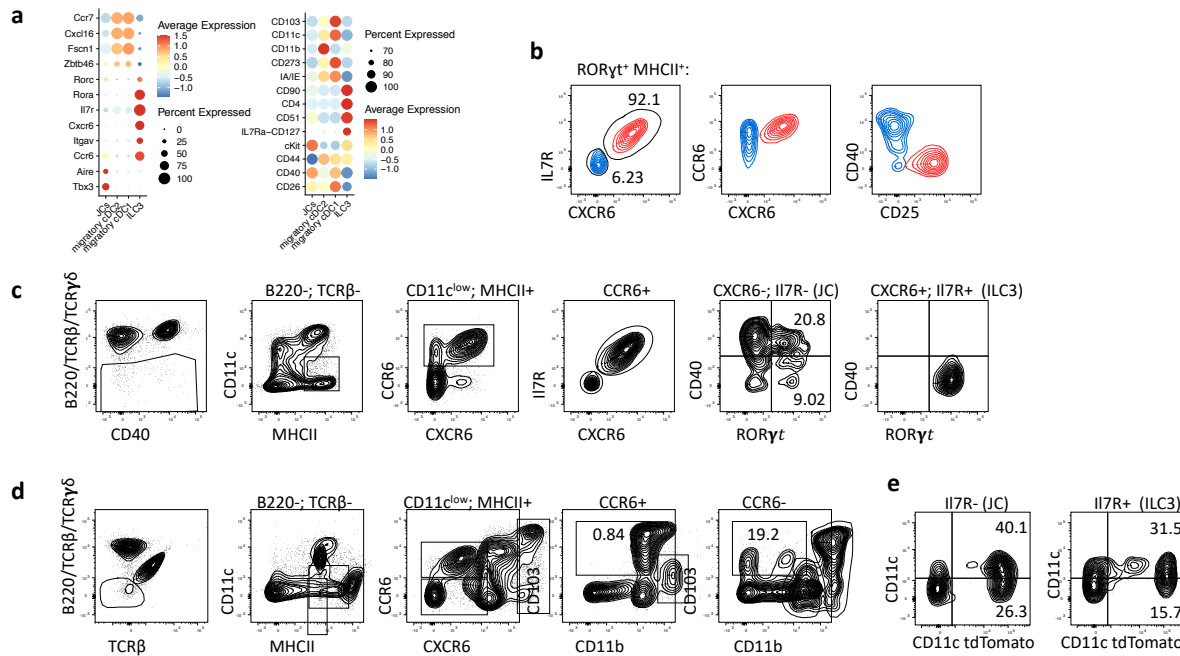
556



557

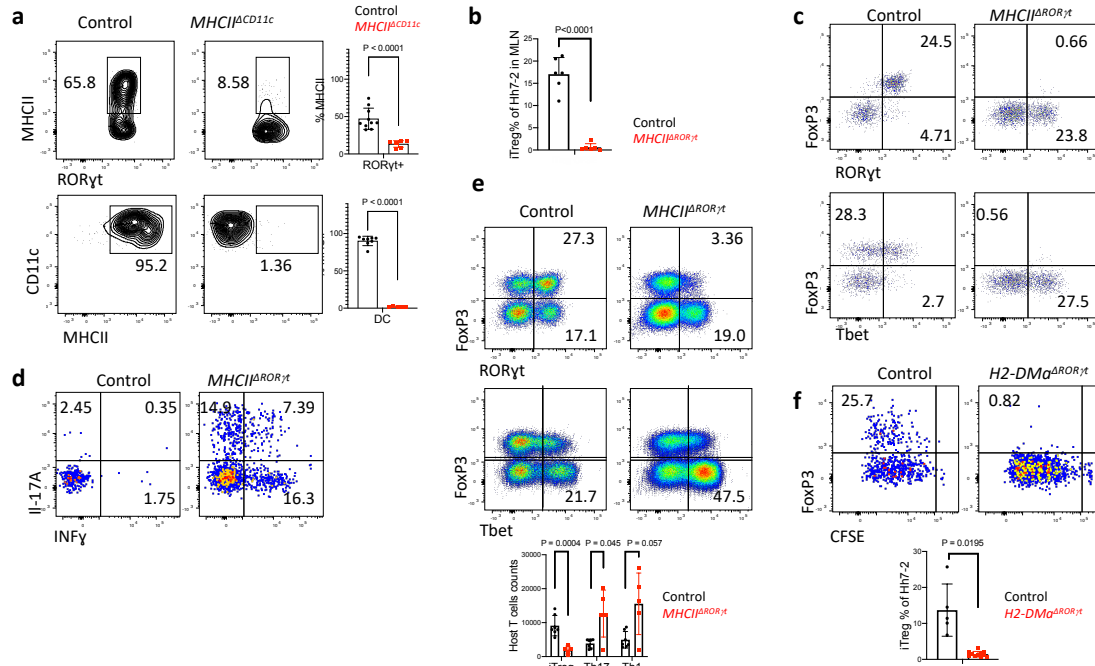
558 **Extended Data Fig. 3. Identification of CITE-seq-assigned clusters of sorted *tdTomato*-**
 559 ***ON*^{ΔCD11c} fate-mapped cells.** **a**, Stacked violin plots for selected (curated) and top DEG (data-
 560 driven) of *tdTomato*⁺ cells sorted from MLN of Hh-colonized mice. **b**, Ridge Plot of cell surface
 561 markers for each cluster.

562



563

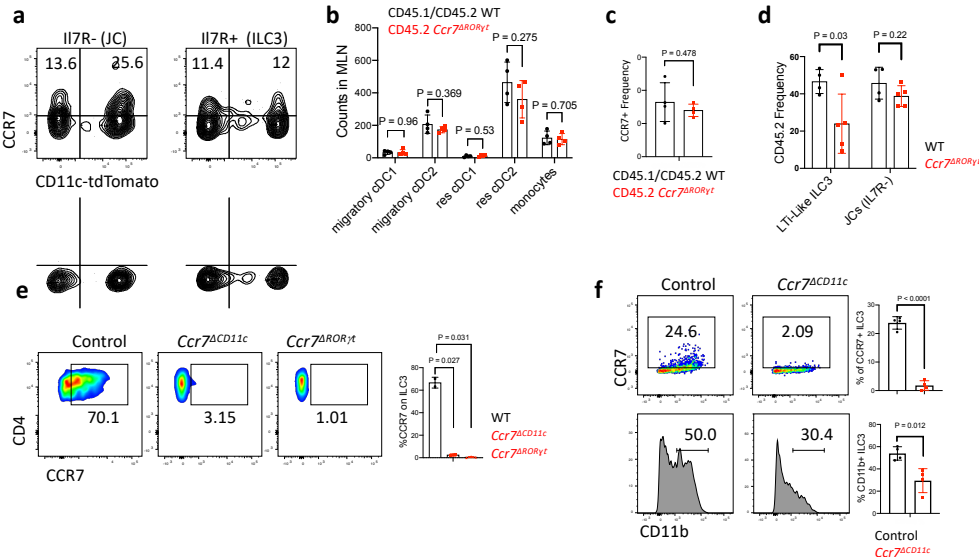
564 **Extended Data Fig. 4. Phenotypic discrimination of ILC3 and JC.** **a**, Dot plots for selected
 565 (curated) DEG and cell surface markers for the indicated clusters, obtained from CITE-seq
 566 analysis of $tdTomato-ON^{CD11c}$ fate-mapped cells. **b**, Flow cytometry profiling of CXCR6,
 567 CD127(IL-7R), CCR6 CD25 and CD40 on ILC3 (red) and JC (blue), pre-gated on TCR β $^-$,
 568 TCR γ δ $^-$, B220 $^-$, ROR γ t $^+$, MHCII $^+$. **c**, gating strategy for JC using cell surface staining as
 569 indicated. **d**, Flow cytometry profiling of JC and DC markers, showing that migratory cDC are
 570 excluded from CD11c low CCR6 $^+$ gating. **e**, TdTomato levels in ILC3 (TCR β $^+$, TCR γ δ $^+$, B220 $^+$,
 571 MHCII $^+$ CCR6 $^+$, II7R $^+$) and JC (TCR β $^+$, TCR γ δ $^+$, B220 $^+$, MHCII $^+$ CCR6 $^+$, II7R $^+$) from the MLN of
 572 Hh-colonized $tdTomato-ON^{CD11c}$ fate-map mice.



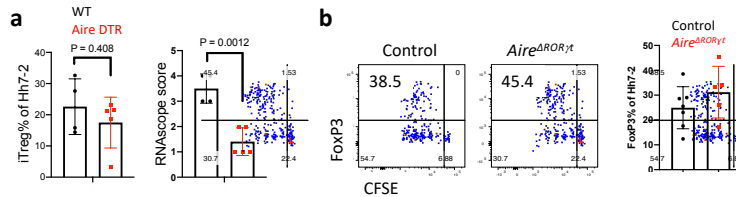
573

574 **Extended Data Fig. 5. Antigen presentation by ROR γ t⁺ cells is required for microbiota-
575 induced iTreg cell differentiation. a, MHCII expression in ROR γ t⁺ cells (top) and DC (bottom)
576 from the MLN of Hh-colonized $MHCII^{\Delta CD11c}$ mice (n=6 and 5) and littermate controls (n =10 and
577 8). ROR γ t⁺ cells were gated as TCR β ⁻, TCR $\gamma\delta$ ⁻, B220⁻, ROR γ t⁺; DC were gated as TCR β ⁻,
578 TCR $\gamma\delta$ ⁻, B220⁻, CD90⁻, CD11c^{high}. b, Bar graph showing frequency of iTreg among Hh7-2 T
579 cells, measured as in Figure 2e. c-d, Representative dot plots showing Hh7-2 T cell
580 differentiation (c) and cytokine (d) profiles in colon lamina propria at 22 days after adoptive
581 transfer into Hh-colonized $MHCII^{\Delta ROR\gamma t}$ and littermate controls. e, Representative and aggregate
582 data of transcription factor profiles of host CD4⁺ T cells in colon lamina propria of mice shown in
583 (c) and (d). f, Hh7-2 cell proliferation and differentiation in the MLN of $H2-DMA^{\Delta ROR\gamma t}$ (ROR γ t-Cre;
584 $H2-Dma^{ff}$) (n=11) and littermate controls (ROR γ t-Cre; $H2-DMA^{ff}$) (n=5) at 3 days after transfer
585 of CFSE labeled naïve Hh7-2, cell proliferation and FoxP3 were assessed in cells isolated from
586 C1 MLN. Representative flow cytometry (left) and aggregate data from multiple animals (right).**

587 Data summarize two independent experiments. All statistics were calculated by unpaired two-
588 sided Welch's t-test. Error bars denote mean \pm s.d. *p*-values are indicated in the figure.
589



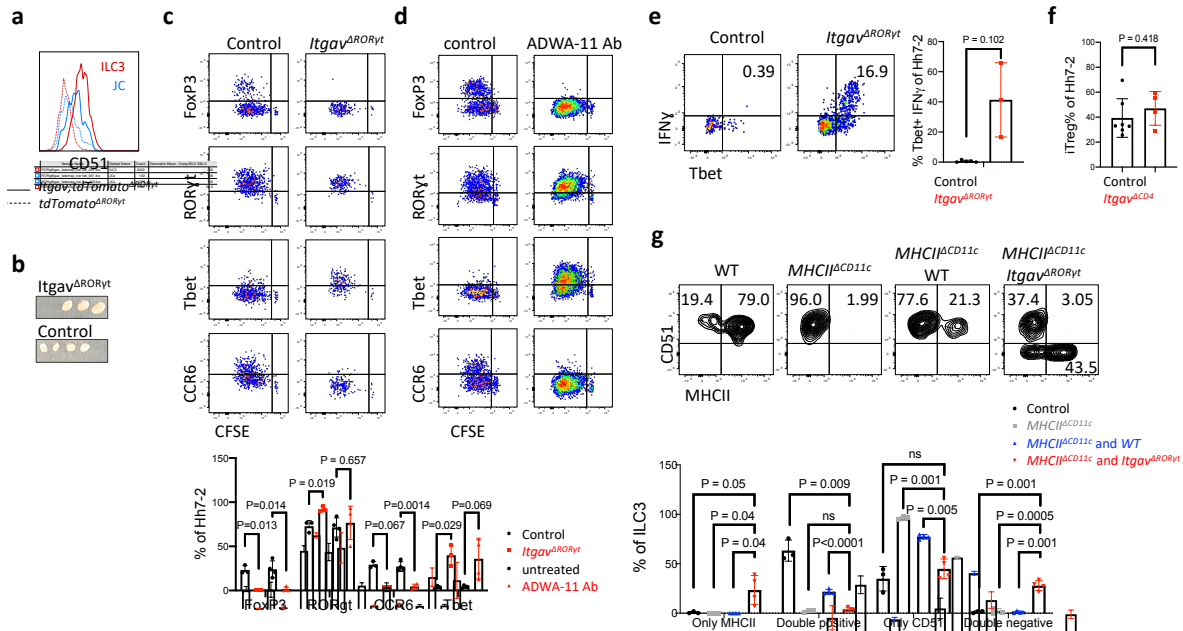
590
 591 **Extended Data Fig. 6. Differential requirements for CCR7 in iTreg and effector Th17 cell**
 592 **differentiation. a,** Cell surface expression of CCR7 on CD11c-Cre fate-mapped ILC3 (TCR β^- ,
 593 TCR $\gamma\delta^-$, B220 $^-$, MHCII $^+$, CCR6 $^+$, IL-7R $^+$) and JC (TCR β^- , TCR $\gamma\delta^-$, B220 $^-$, MHCII $^+$, CCR6 $^+$, IL-7R $^-$)
 594 in the MLN. **b-c,** Analysis of DC counts in MLN (b) and large intestine (c) of WT and *Ccr7ΔRORyt*
 595 mixed bone marrow chimeric mice described in Figure 3c. Counts in the MLN of DC subsets
 596 derived from bone marrow (b); frequencies of CCR7 $^+$ among total colonic DCs (c) (n=4).
 597 Statistics were calculated using paired two-sided t-test. **d,** Analysis of CD45.2 frequencies within
 598 donor cells is presented for ILC3 (TCR β^- , TCR $\gamma\delta^-$, B220 $^-$, MHCII $^+$, ROR γt^+ , IL-7R $^+$) and JC
 599 (TCR β^- , TCR $\gamma\delta^-$, B220 $^-$, MHCII $^+$, ROR γt^+ , IL-7R $^-$) in the MLN of WT and *Ccr7ΔRORyt* mixed bone
 600 marrow chimeric mice described in Figure 3c. **e,** Cell surface expression of CCR7 in colonic
 601 ILC3 (TCR β^- , TCR $\gamma\delta^-$, B220 $^-$, CD90 $^+$, ROR γt^+ , CD25 $^+$, CD4 $^+$) from *Ccr7ΔRORyt* (n=3), *Ccr7ΔCD11c*
 602 (n=2) and control Hh-colonized mice (n=2). **f,** Cell surface expression of CCR7 and CD11b in
 603 ILC3-gated MLN cells (TCR β^- , TCR $\gamma\delta^-$, B220 $^-$, IL-7R $^+$, CCR6 $^+$, CD25 $^+$) from *Ccr7ΔCD11c* (n=4) and
 604 control Hh-colonized mice (n=4).



605

606 **Extended Data Fig. 7. Analysis of Aire⁺ JC function in differentiation of Hh-specific iTreg**

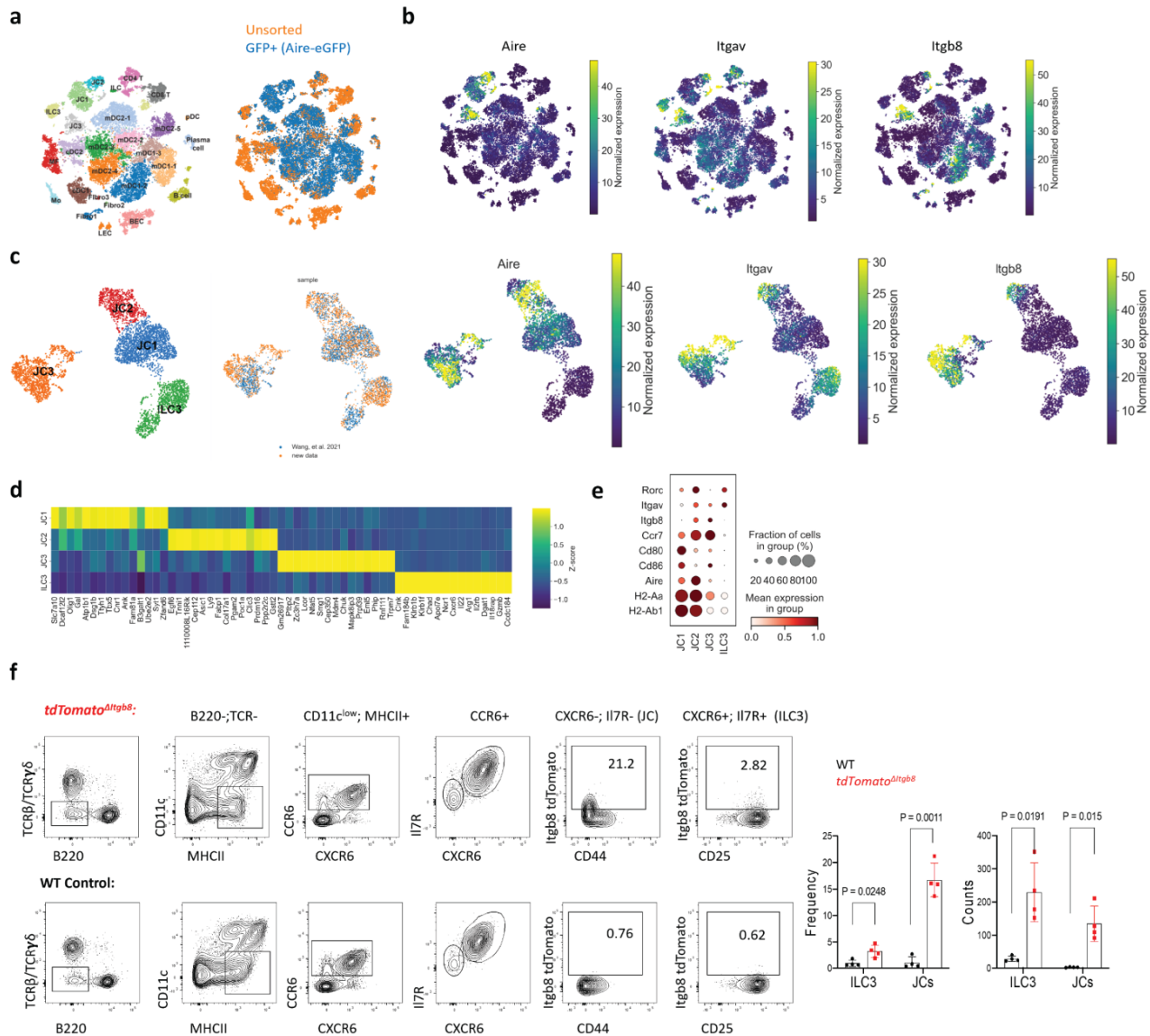
607 **cells. a**, Lethally irradiated mice were reconstituted with BM cells from CD45.2 *Aire-DTR* or
608 CD45.2 WT mice. One month after reconstitution, mice were colonized with Hh, and one week
609 later were treated with Diphtheria toxin (DT, Sigma-Aldrich) for 3 sequential days (at a dose of
610 25 ng/g mice). CD45.1/CD45.2 CFSE-labeled Hh7-2 T cells (1×10^5) were transferred
611 intravenously into the mice on the first day of DT treatment. Bar graph of proportion of
612 proliferating Foxp3⁺ Hh7-2 T cells in the MLN of mice reconstituted with *Aire-DTR* BM (n=5) or
613 with WT BM (n=4) (left); *Aire* mRNA in the spleen of the treated mice was blindly scored using
614 RNA scope analysis. **b**, Proliferation and differentiation of CFSE-labeled Hh7-2 T cells in the
615 MLN of *ROR γt -Cre;Aire^{ff}* (n=5) and control *Aire^{ff}* littermates (n=7) at 3 days after adoptive
616 transfer. Data summarize three independent experiments. All statistics, except for b and c, were
617 calculated by unpaired two-sided Welch's t-test. Error bars denote mean \pm s.d. p-values are
618 indicated in the figure.



619

620 **Extended Data Fig. 8. Effect of integrin $\alpha_v\beta_8$ blockade or α_v inactivation on microbiota-
621 dependent T cell differentiation.** **a**, Expression of integrin α_v (CD51) in fate-mapped ROR γ^t
622 cell subsets from MLN of wild type and *Itgav*^{ACD11c} mice. **b**, C1 MLN from *Itgav*^{ACD11c} (n=3) and
623 littermate controls (n=4), 10 days after Hh colonization. **c-d**, Flow cytometry profiling of
624 transcription factors and CCR6 in proliferating CFSE-labeled Hh7-2 in the MLN at 3 days after
625 adoptive transfer into *Itgav*^{ACD11c} (n=3) and littermate control mice (n=3) (b) or into mice treated
626 with ADWA11(n=4) (as in Fig. 4a) or untreated control littermates (n=4) (c). Summary data of
627 results in (b) and (c) are shown below. **e**, Intracellular IFN γ and T-bet expression in
628 PMA/Ionomycin-stimulated Hh7-2 T cells isolated from colon lamina propria of *Itgav*^{ACD11c}(n=3)
629 and control littermates (n=5), 10 days after adoptive transfer. **f**, Frequency of iTreg cells among
630 proliferating Hh7-2 in the MLN at 3 days after adoptive transfer into *Itgav*^{ACD4} (n=4) and control
631 littermates (n=7). Data summarize two independent experiments. **g**, Integrin α_v and MHCII cell
632 surface expression in ILC3 (gated as TCR β^- , TCR $\gamma\delta^-$, B220 $^-$, ROR γ^t $^+$, CD90 $^+$, CD25 $^+$ CD45.2 $^+$)
633 isolated from MLN of bone marrow chimeric mice, reconstituted with different combinations of

634 donor cells as indicated and colonized with Hh for 10 days. Data summarized below for control
635 ($n=3$), $MHCII^{4CD11c}$ ($n=3$), $MHCII^{4CD11c}$ and WT ($n=4$), and $MHCII^{4CD11c}$ and $Itgav^{4ROR\gamma t}$ ($n=4$)
636 reconstituted mice. All Statistics were calculated by unpaired two-sided Welch's t-test. Error
637 bars denote mean \pm s.d. p -values are indicated in the figure.
638

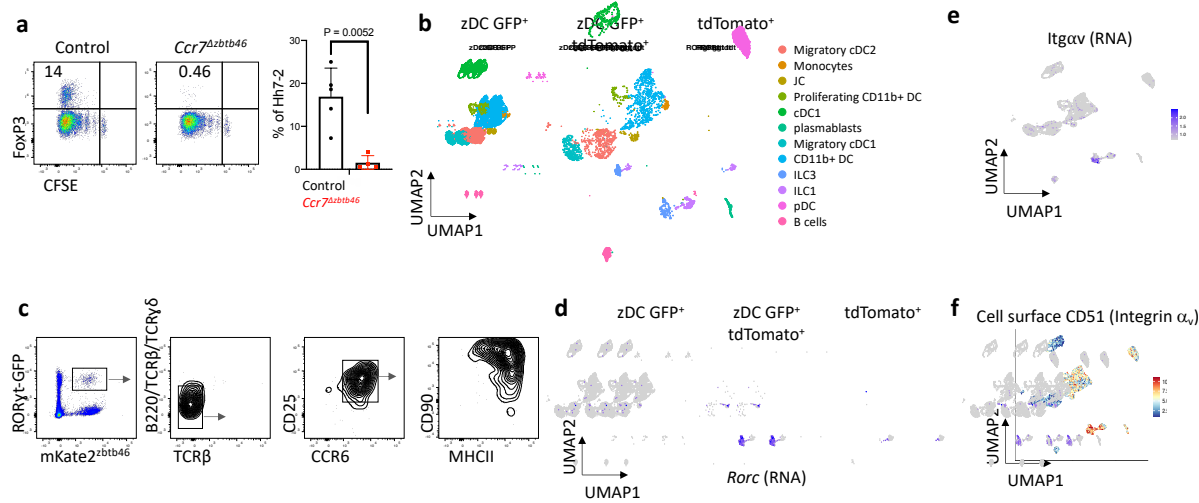


639

640 **Extended Data Fig. 9. *Itgav* and *Itgb8* expression in ILC3 and JC.** **a**, tSNE plot with Leiden
 641 clustering of scRNAseq of pooled GFP⁺ sorted and unsorted cells, as indicated, from pooled
 642 lymph nodes of Adig mice³². **b**, tSNE feature plots showing *Aire*, *Itgav*, and *Itgb8* levels in the
 643 cell clusters. **c**, UMAP plot of *Aire*+ JC and ILC3 populations from pooled datasets as indicated
 644 with associated feature plots. **d**, top differentially expressed genes per pseudobulk cluster in (c),
 645 shown by heatmap. **e**, dot plot of selected genes in JC and ILC3 clusters. **f**, Representative flow
 646 cytometry (left) and aggregate results (right) of tdTomato⁺ JC and ILC3, gated as indicated, in

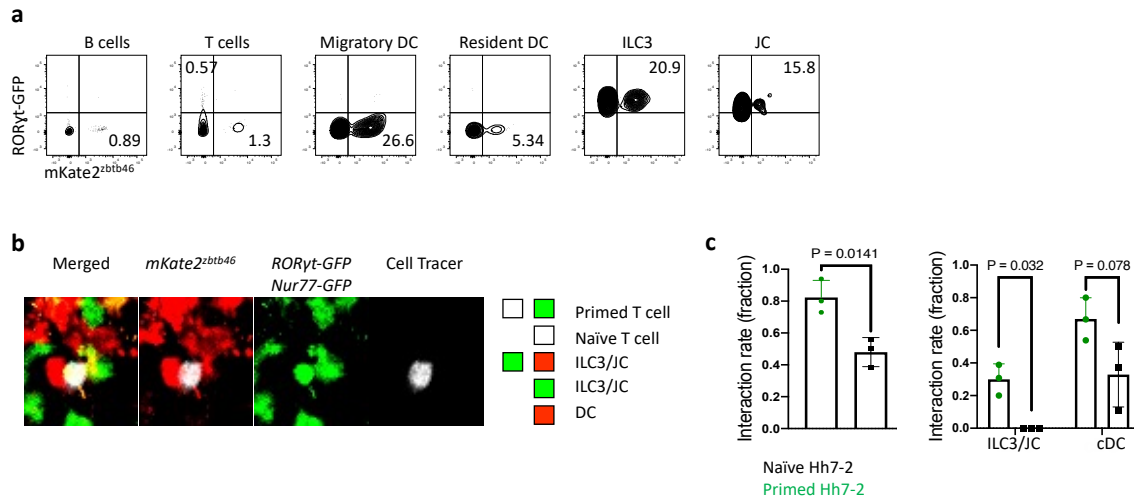
647 C1 MLN of *tdTomato*^{Δ $lgb8$} mice³³ (n=4) and littermate controls (n=4). Aggregate data (right) show
648 percent tdTomato+ cells among total ILC3 and JC and number of reporter-positive cells in the
649 C1 MLN of each mouse. All statistics were calculated by unpaired two-sided Welch's t-test.
650 Error bars denote mean ± s.d. *p*-values are indicated in the figure.
651

652



653

654 **Extended Data Fig. 10. Analysis of ROR γ t-expressing cells in the MLN. a, Hh7-2**
655 proliferation and differentiation in MLN of *Ccr7*^{Δzbtb46} (n= 4) and control littermates (n=5), at 3
656 days after transfer of the naïve cells. Data in the right panel summarize three independent
657 experiments. **b**, UMAP visualization of CITE-seq datasets obtained from 3 distinct sorted
658 populations (GFP⁺, GFP⁺ tdTomato⁺ and tdTomato⁺) isolated from C1 MLN of *Zbtb46-eGFP* ;
659 *tdTomato-ON*^{ΔROR γ t} mice (n=2), analyzed by the WNN method. **c**, Flow cytometry analysis of
660 fate-mapped C1 MLN cells from *ROR γ t-eGFP;mKate2-ON*^{Δzbtb46} mice, gated for the indicated
661 cell subsets. **d-e**, Feature plot showing *Rorc* (d) and integrin α_v (e) levels in the cell clusters
662 identified in the CITE-seq analysis shown in (b); Positive cells are layered in front. All statistics
663 were calculated by unpaired two-sided Welch's t-test. Error bars denote mean \pm s.d. *p*-values
664 are indicated in the figure.



665

666 **Extended Data Fig. 11. Intravital tracking of ROR γ t-expressing cells and DC interactions**

667 **with Hh-specific T cells during priming in the MLN. a, Flow cytometry analysis of fate-**

668 **mapped C1 MLN cells from $ROR\gamma$ t-eGFP; $mKate2$ -ON zbtb46 mice, gated for the indicated cell**

669 **subsets (ILC3 were gated as TCR β $^-$, TCR $\gamma\delta$ $^-$, B220 $^-$, MHCII $^+$, ROR γ t-eGFP $^+$, CCR6 $^+$, CD25 $^+$ and**

670 **JC as TCR β $^-$, TCR $\gamma\delta$ $^-$, B220 $^-$, MHCII $^+$, ROR γ t-eGFP $^+$, CD25 $^-$). Note that there is incomplete**

671 **excision of the transcriptional stop signal by $zbtb46$ -Cre. b, Representative image of cell-cell**

672 **interactions of recently primed Hh-specific T cells with DC and ROR γ t-expressing cells. $Nur77$ -**

673 **eGFP tracer-labeled Hh7-2 T cells were transferred into of $ROR\gamma$ t-eGFP; $mKate2$ -ON zbtb46 Hh-**

674 **colonized mice. Cell colocalization of primed Hh7-2 (tracer dye $^+$, GFP $^+$) or naïve Hh7-2 (tracer**

675 **dye $^+$, GFP $^-$) T cells with cDC ($mKate2^+$ with dendritic morphology), ROR γ t-expressing cells**

676 **(eGFP $^+$, $mKate2^+$ or eGFP $^+$ alone with amoeboid morphology), or both were visualized using**

677 **intravital multiphoton microscopy of the C1 MLN at 15 h after transfer. Note that Cell Tracer**

678 **fluorescent labeling provides clear spatial discrimination of $ROR\gamma$ t-eGFP and $Nur77$ -eGFP**

679 **expressing cells. c, Quantification and graphical representation of the total and individual rates**

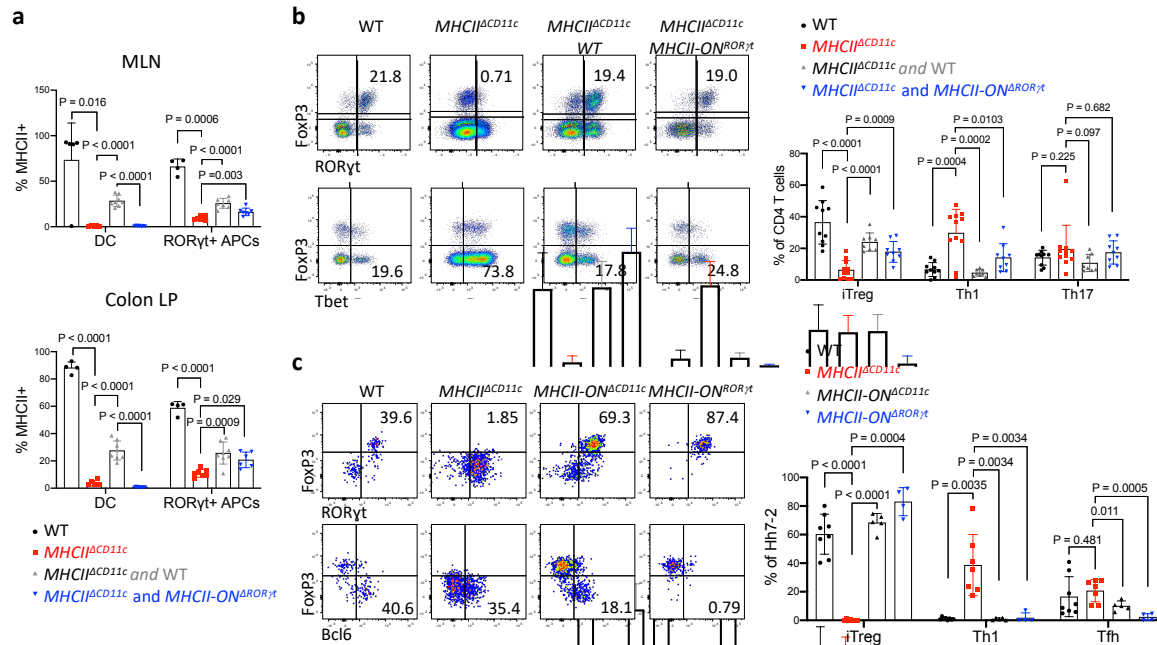
680 **of interaction of ROR γ t-expressing cells or cDC populations with primed or naïve Hh7-2 T**

681 **cells. Data summarize cell-cell interactions from six 0.25mm 3 three-dimensional regions of C1**

682 **MLN, (n=72 total Hh7-2 T cells), (n=49 primed and 23 naïve Hh7-2 T cells). All statistics were**

683 calculated by unpaired two-sided Welch's t-test. Error bars denote mean \pm s.d. *p*-values are
684 indicated in the figure.

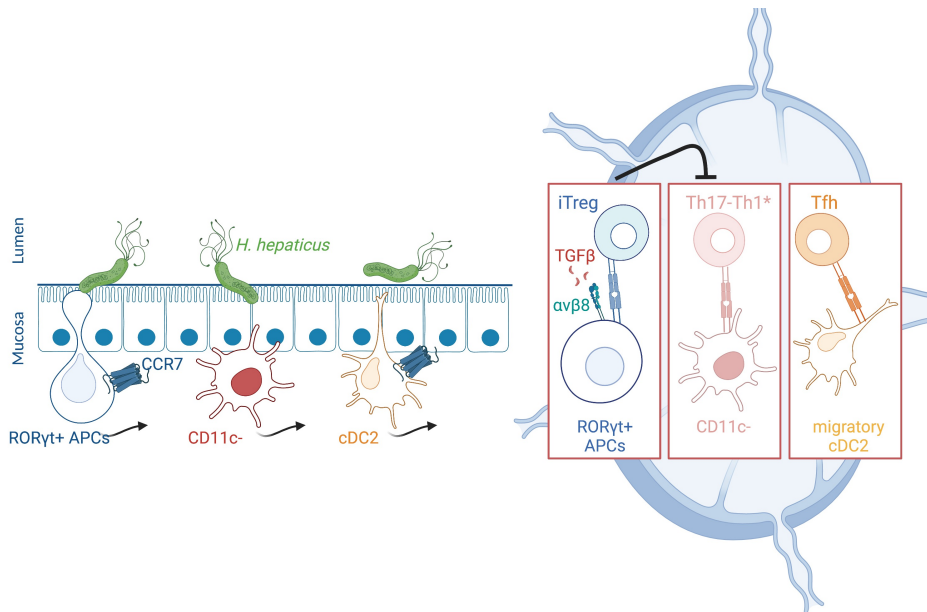
685



686

687 **Extended Data Fig. 12. Gain-of-function expression of MHCII in ROR γ t⁺ cells rescues**
 688 **bone marrow-derived iTreg cell differentiation.** **a**, Aggregate data showing MHCII frequency
 689 on donor-derived DC and ROR γ t⁺ cells in MLN and colon lamina propria from chimeric mice
 690 reconstituted with combinations of donor BM cells as indicated, with representative flow
 691 cytometry panel in Fig. 5b. MLN: WT (n=5), $MHCII\Delta CD11c$ (n=5), $MHCII\Delta CD11c$ and WT (n=8),
 692 $MHCII\Delta CD11c$ and $MHCII-ON\Delta ROR\gamma t$ (n=7). Colon: WT (n=4), $MHCII\Delta CD11c$ (n=6), $MHCII\Delta CD11c$ and
 693 WT (n=8), $MHCII\Delta CD11c$ and $MHCII-ON\Delta ROR\gamma t$ (n=6). **b**, Donor bone marrow-derived CD4⁺ T cell
 694 differentiation in colon lamina propria from chimeric mice reconstituted with combinations of BM
 695 cells as indicated. Representative flow panels (left) and aggregate data (right). WT (n=10),
 696 $MHCII\Delta CD11c$ (n=11), $MHCII\Delta CD11c$ and WT (n=8), $MHCII\Delta CD11c$ and $MHCII-ON\Delta ROR\gamma t$ (n=9). Colon:
 697 WT (n=4), $MHCII\Delta CD11c$ (n=6), $MHCII\Delta CD11c$ and WT (n=8), $MHCII\Delta CD11c$ and $MHCII-ON\Delta ROR\gamma t$ (n=7).
 698 **c**, Representative flow cytometry (left) and aggregate data (right) of Hh7-2 T cell differentiation
 699 in colon lamina propria of Hh-colonized bone marrow chimeric mice reconstituted with cells of
 700 indicated genotypes, 12 days after transfer of naive TCR transgenic T cells. WT (n=8),

701 $MHCII^{\Delta CD11c}$ (n=7), $MHCII-ON^{\Delta CD11c}$ (n=5), and $MHCII-ON^{\Delta RORyt}$ (n=4). Data summarize two or
702 three independent experiments. All statistics were calculated by unpaired two-sided Welch's t-
703 test. Error bars denote mean \pm s.d. *p*-values are indicated in the figure.
704



705

706 **Extended Data Fig. 13. Schematic of the requirement of distinct APC subsets for T cell**
707 **differentiation.** CCR7 and integrin $\alpha_v\beta_8$ are required in ROR γ t⁺ APCs for iTreg cell
708 differentiation. Note that other APCs, with differential requirements for CCR7 expression, are
709 involved in the priming and differentiation of pathogenic Th17 and Tfh cells.

710

711

712

713

714 **Methods**

715

716 **Mice**

717 Mice were bred and maintained in the Alexandria Center for the Life Sciences animal facility of
718 the New York University School of Medicine, in specific pathogen-free conditions. C57BL/6 mice
719 (Jax# 000664), *Batf3*^{-/-} (B6.129S(C)-*Batf3tm1Kmm*/J #Jax 013755), *Itgav*^{ff} (B6.129P2(Cg)-
720 *Itgav*^{tm2Hyn}/J Jax# 032297, CD45.1 mice (B6.SJL-*Ptprrca Pepcb*/BoyJ, Jax# 002014), *CD4-Cre*
721 (*Tg(Cd4-cre)1Cwi*/BfluJ, Jax# 017336), *CD11c-Cre* (B6.Cg-*Tg(Itgax-cre)1-1Reiz*/J #Jax 008068),
722 *Ccr7*^{-/-} (B6.129P2(C)-*Ccr7tm1Rfor*/J, Jax# 006621), *I-AB*^{ff} (B6.129X1-H2-*Ab1tm1Koni*/J #Jax
723 013181), *Zbtb46-Cre* (B6.Cg-*Zbtb46tm3.1(cre)Mnz*/J #Jax 028538), *Zbtb46-eGFP*
724 (B6.129S6(C)-*Zbtb46tm1.1Kmm*/J #Jax 027618), *tdTomato*^{LSL} (B6.129S6-
725 *Gt(ROSA)26Sortm14(CAG-tdTomato)Hze*/J #Jax 007908), *Aire*^{ff} (B6.Cg-*Airetm1Dfil*/J #Jax
726 031409), *Nur77-eGFP* (C57BL/6-*Tg(Nr4a1-EGFP/cre)820Khog*/J #Jax 016617), *CD90.1* (B6.*PL-*
727 *Thy1a*/CyJ #Jax 000406) mice were purchased from Jackson Laboratories. *RORyt-Cre* and *Hh7-*
728 *2tg* were generated in our laboratory and previously described^{3,39}. BAC-transgenic *Rorc(t)-GfpTG*
729 were generated by G. Eberl's lab⁴⁰. *huLangerin* (*CD207*)-*DTA* mice were kindly provided by
730 Daniel H. Kaplan⁴¹. *Ccr7*^{ff} mice were previously described¹⁴. *mKate2*^{LSL} mice⁴² were provided by
731 Scott Lowe. *I-AB* *lox*-*STOP*-*lox*³⁵, *Aire*-*DTR*⁴³, *H2-DMa1*^{ff}²³, *Itgb8-tdTomato*³³ Adig (Aire-Driven
732 *Igrp-Gfp*)³² mice have been described. Littermates with matched sex (both males and females)
733 were used. Mice in all the experiments were 6–12 weeks old at the starting point of treatment.
734 Animal sample size estimates were determined using power analysis (power=90% and
735 alpha=0.05) based on the mean and standard deviation from our previous studies and/or pilot
736 studies using 4–5 animals per group. All animal procedures were performed in accordance with
737 protocols approved by the Institutional Animal Care and Usage Committee of New York University
738 School of Medicine.

739

740

741 **Antibodies, intracellular staining and flow cytometry**

742 The following monoclonal antibodies were purchased from eBiosciences, BD Pharmingen or
743 BioLegend: CD3 (145-2C11), CD4 (RM4-5), CD25 (PC61), CD44 (IM7), CD45.1 (A20), CD45.2
744 (104), CD90.1 (HIS51), CD90.2 (53-2.1), CD19 (1D3), CD45R (RA3-6B2), CD127 (A7R34), CD51
745 (RMV-7), IA/IE (56-5321-82), CCR6 (3D6), Ncr1 (29A1.4), NK1.1 (PK136), CD62L (MEL-14),
746 CXCR5 (L138D7), TCR β (H57-597), TCR V β 6 (RR4-7), Bcl-6 (K112-91), Foxp3 (FJK-16s),
747 ROR γ t (B2D or Q31-378), T-bet (eBio4B10), IL-17A (eBio17B7) and IFN- γ (XM61.2), CD11c
748 (N418), CD11b (M1/70), CX3CR1 (SA011F11), Ly6c (HK1.4), SIRPa (P84), Ly6G (1A8), CD273
749 (TY25), Clec12a (5D3), CD103 (M290), XCR1 (ZET), F4/80 (BM8), CCR7 (4B12), CXCR6
750 (SA051D1), CD40 (HM40-3), 4',6-diamidino-2-phenylindole (DAPI) or Live/dead fixable blue
751 (ThermoFisher) was used to exclude dead cells.

752 For transcription factor staining, cells were stained for surface markers, followed by fixation and
753 permeabilization before nuclear factor staining according to the manufacturer's protocol (Foxp3
754 staining buffer set from eBioscience). For cytokine analysis, cells were incubated for 5 h in RPMI
755 with 10% FBS, phorbol 12-myristate 13-acetate (PMA) (50 ng/ml; Sigma), ionomycin (500 ng/ml;
756 Sigma) and GolgiStop (BD). Cells were stained for surface markers before fixation and
757 permeabilization, and then subjected to intracellular cytokine staining according to the
758 manufacturer's protocol (Cytofix/Cytoperm buffer set from BD Biosciences). Flow cytometric
759 analysis was performed on an LSR II (BD Biosciences) or Cytek Aurora (Cytek) or an Aria II (BD
760 Biosciences) and analyzed using FlowJo software (Tree Star).

761

762 **Flow cytometry gating strategy**

763 **Hh7-2 gating:** FSC, SSC; Live Dead $^-$, singlets, Dump $^-$ (B220, TCRgd, Ly6G), MHCII $^-$, CD4 $^+$,
764 TCR β $^+$, VB6 $^+$, CD45.1 $^+$ or CD90.1 $^+$; **cDC gating:** FSC, SSC; Live Dead $^-$, singlets, Dump $^-$ (B220,
765 TCR β , TCRgd, Ly6G), CD11c $^+$ and CD11b $^+$, SIRPa $^{\text{low-moderate}}$ (remove CD11c $^-$, SIRPA $^{\text{high}}$); **cDC2**

766 **gating** (unless mentioned otherwise): FSC, SSC; Live Dead⁻,singlets, Dump⁻ (B220,TCRgd,
767 Ly6G), CD11c⁺ and CD11b⁺ , SIRPa^{low-moderate} (remove CD11c⁻, SIRPA^{high}), Clec12a⁻ SIRPa⁺;
768 **migratory cDC2 gating**: FSC, SSC; Live Dead⁻,singlets, Dump⁻ (B220,TCRgd, Ly6G), CD11c⁺
769 and CD11b⁺ , SIRPa^{low-moderate} (remove CD11c⁻, SIRPA^{high}), Clec12a⁻ SIRPa⁺, PDL2⁺; **NCR1⁺ ILC3**
770 **gating**: FSC, SSC; Live Dead⁻,singlets, Dump⁻ (B220,TCRgd, Ly6G), TCR β ⁻ , CD90+, II7R⁺,
771 ROR γ t⁺, CCR6⁻, NCR1⁺; **JC** (using internal staining): FSC, SSC; Live Dead⁻,singlets, Dump⁻
772 (B220,TCRgd, Ly6G), TCR β ⁻ , ROR γ t⁺, MHCII+ CXCR6⁻, II7R⁻; **JC** (excluding internal staining):
773 FSC, SSC; Live Dead⁻,singlets, Dump⁻ (B220,TCRgd, Ly6G), TCR β ⁻ , CD11c^{low-negative}, MHCII⁺,
774 CCR6⁺,CXCR6⁻, II7R⁻ ; **ILC3**: FSC, SSC; Live Dead⁻,singlets, Dump⁻ (B220,TCRgd, Ly6G),
775 TCR β ⁻ , CXCR6⁺, II7R⁺, ROR γ t⁺; **LTi-Like ILC3** (using internal staining): FSC, SSC; Live Dead⁻
776 ,singlets, Dump⁻ (B220,TCRgd, Ly6G), TCR β ⁻ , MHCII+ CXCR6⁺, II7R⁺, ROR γ t⁺, CCR6⁺, CD25⁺;
777 **LTi-Like ILC3** (excluding internal staining): FSC, SSC; Live Dead⁻,singlets, Dump⁻ (B220,TCRgd,
778 Ly6G), TCR β ⁻ , CD11c^{low-negative}, MHCII⁺, CCR6⁺,CXCR6⁺, II7R⁺
779

780 **Isolation of lymphocytes and APCs**

781 After removal of caecal patches, large intestine tissues were sequentially treated with PBS
782 containing 1 mM DTT at room temperature for 10 min, twice with 5 mM EDTA at 37 °C for 10 min
783 to remove epithelial cells, and then minced and dissociated in digestion buffer (RPMI containing
784 collagenase (1 mg ml⁻¹ collagenase D; Roche), DNase I (100 µg ml⁻¹; Sigma), dispase (0.1 U
785 ml⁻¹; Worthington) and 10% FBS) with constant stirring at 37 °C 55 min. Leukocytes were
786 collected at the interface of a 40%/80% Percoll gradient (GE Healthcare). Lymph nodes were
787 mechanically disrupted for lymphocyte isolation. For isolation of myeloid cells and ILC, lymph
788 nodes were mechanically disrupted with digestion buffer with constant stirring at 37 °C 30 min.

789

790 ***H. hepaticus* culture and oral infection**

791 *H. hepaticus* was kindly provided by Dr. James Fox (MIT). Hh was cultured and administrated as
792 was previously described³. Frozen stock aliquots of *H. hepaticus* were stored in Brucella broth
793 with 20% glycerol and frozen at -80°C. The bacteria were grown on blood agar plates (TSA with
794 5% sheep blood, Thermo Fisher). Inoculated plates were placed into a hypoxia chamber (Billups-
795 Rothenberg), and anaerobic gas mixture consisting of 80% nitrogen, 10% hydrogen, and 10%
796 carbon dioxide (Airgas) was added to create a micro-aerobic atmosphere, in which the oxygen
797 concentration was 3~5%. The micro-aerobic jars containing bacterial plates were left at 37°C for
798 4 days before animal inoculation. For oral infection, *H. hepaticus* was resuspended in Brucella
799 broth by application of a pre-moistened sterile cotton swab applicator tip to the colony surface.
800 0.3 mL bacterial suspension was administered to each mouse by oral gavage. Mice were
801 inoculated for a second dose after 3 days.

802

803 **Adoptive transfer of Hh7-2 TCR transgenic cells**

804 Adoptive transfer of Hh7-2 was done as was previously described³, with minor modifications.
805 Recipient mice were colonized with *H. hepaticus* by oral gavage seven days before adoptive
806 transfer. Spleens and lymph nodes from donor Hh7-2 TCRtg mice were collected and
807 mechanically disassociated. Red blood cells were lysed using ACK lysis buffer (Lonza). Naive
808 Hh7-2 T cells were sorted as CD4⁺TCR β ⁺CD44^{lo}CD62L^{hi}CD25⁻V β 6⁺ (HH7-2tg), on the Aria II (BD
809 Biosciences). For analysis of early differentiation, cells were additionally labeled with CFSE
810 (ThermoFisher). Cells were resuspended in PBS on ice and 100K were transferred into congenic
811 isotype-labelled recipient mice by retro-orbital injection. Cells from MLN were analyzed 3 days
812 after transfer and cells from colon LP were analyzed 10-14 days after transfer.

813

814 **CITE-seq**

815 CITE-seq and cell hashing were performed as described^{44,45} with minor modifications. Single-cell
816 suspensions were obtained from digests of C1 MLN of *tdTomato-ON*^{CD11c} or *tdTomato-ON*^{ROR γ t};
817 *zbtb46-eGFP* mice that had been colonized with *Helicobacter* for 7 days. Cells were sorted on a
818 BD FACSAriall using a 100- μ m nozzle. Dead cells as well as T cells and B cells were gated out
819 using DAPI, TCR β , TCR $\gamma\delta$ and B220 antibodies. From *tdTomato-ON*^{CD11c} mice, the *tdTomato*⁺
820 population was collected separately from two mice. From *tdTomato-ON*^{ROR γ t}; *zbtb46-eGFP* mice,
821 we collected 3 populations from two separate mice: GFP⁺, GFP⁺ *tdTomato*⁺ and *tdTomato*⁺.
822 Sorted cells were stained separately with hashing antibodies (Biolegend)⁴⁵. After removal of
823 excess hashing antibodies, we combined the samples and stained them with CITE-seq
824 antibodies, conjugated using iEDDA click chemistry to barcode oligos as described before⁴⁶. In
825 addition, we included some commercially available Totalseq-A antibodies for CD11c, CD90.2,
826 CD185, CD51 and CD127 (Biolegend). Post-sorting and staining, cells were run through the
827 standard 10x Chromium (v3) protocol up until cDNA amplification, with the following modification:
828 For the cDNA PCR step, 0.2uM of ADT additive primer (5'CCTTGGCACCCGAGAATTCC) and
829 0.2uM of HTO additive primer (5'GTGACTGGAGTTCAGACGTGTGCTC) were added to the
830 cDNA amplification master mix. Post cDNA amplification, a 0.6X SPRI cleanup was performed to
831 separate the cDNA fraction (on beads) from the smaller ADT and HTO fractions (in supernatant).
832 The cDNA fraction was converted into a 3' tag gene expression library according to the 10x
833 Genomics Single Cell Genomics Protocol (v3). Supernatant from cleanup was kept for ADT and
834 HTO preparation.
835
836 To the supernatant, another 1.4X SPRI was added to bring the total SPRI concentration to 2X.
837 After washing the beads in 80% ethanol and eluting in water, a second round of 2X SPRI cleanup
838 was performed to remove any residual primer carryover from the cDNA PCR. Post cleanup, eluate
839 was taken into ADT PCR amplification (using TruSeq Small RNA RPIx primer

840 (5'CAAGCAGAAGACGGCATACGAGXXXXXXXXGTGACTGGAGTTCCCTGGCACCCGAGAAT
841 TCCA) and SI PCR primer
842 (5'AATGATACGGCGACCACCGAGATCTACACTCTTCCCTACACGACGCTC), and into
843 hashtag amplification (using TruSeq D7xx
844 (5'CAAGCAGAAGACGGCATACGAGATXXXXXXXXGTGACTGGAGTCAGACGTGTGC) and
845 SI PCR primers). Libraries were pooled and sequenced on a 100 cycle Novaseq S1 flowcell, with
846 the configuration of 30 base pairs for R1, and 92 base pairs for R2. Additional protocol details can
847 be found for CITE-seq and cell hashing at www.cite-seq.com.

848
849 Post sequencing, gene expression count matrices were generated using cellranger version 5.0
850 using the refdata-gex-mm10-2020-A reference library provided by 10x Genomics, with the
851 additional sequences of cre, eGFP, and tdTomato. Counts matrices for hashtags and antibodies
852 were generated using CITE-seq-Count version 1.4.4. Downstream analysis was then performed
853 in R using Seurat.

854
855 Quality control and doublet removal: We initially selected all cells that were detected in our RNA-
856 seq, cell hashing, and ADT libraries. We removed cells with < 700 detected genes, but also
857 removed cells which had an aberrantly high number of genes (more than 5,000 genes) and a high
858 percentage of mitochondria genes (more than 6%). Additionally, we removed the cells which
859 were attached by the clumps of antibodies and had a too high number of ADT or HTO UMIs (more
860 than 5,000 ADT UMI and 4,000 HTO UMI). We used our previously described hashing-based
861 doublet detection strategy⁴⁵, implemented in HTODemux, to identify doublets that represent two
862 or more cells representing different samples. Only Singlet cells were used for the downstream
863 analysis.

864

865 Multimodal analysis: We normalized RNA data using SCTransform⁴⁷ and applied the centered-
866 log ratio (CLR) transformation to normalize ADT data within each cell. We used principal
867 component analysis (PCA) to reduce dimensionality of both datasets. Then we took both top 20
868 RNA and protein PCA dimensions as the input of weighted nearest neighbors (WNN) method⁴⁸
869 to construct the multimodal weighted KNN graph. To cluster our multimodal dataset, we first used
870 the weighted KNN graph to generate a shared nearest neighbor graph (SNN) and then apply the
871 graph-based smart local moving (SLM) algorithm (<https://doi.org/10.1140/epjb/e2013-40829-0>)
872 on this SNN graph to find clusters with 0.8 resolution. We performed differential expression on all
873 pairs of clusters for both RNA and protein markers, and merged clusters that did not exhibit clear
874 evidence of separation. All samples were clustered together and separated later for further
875 analysis as indicated.

876

877 **CITE-seq data projection in Flowjo**

878 For gating analysis, scaled and normalized ADT counts together with cluster identity, UMAP and
879 UWnn coordinates were exported into a csv format that was uploaded in FlowJo.

880

881 **Single cell RNAseq of Aire⁺ cells**

882 Four week-old Adig mouse lymph nodes (cervical, brachial, axillary, inguinal, and mesenteric)
883 (n=3) were pooled in digestion medium consisting of RPMI 1640 with 2% fetal bovine serum (FBS)
884 (Sigma-Aldrich), deoxyribonuclease (DNase) (100 µg/ml; Roche) and Liberase (50 µg/ml; Roche),
885 minced and agitated at 37°C for 30 min, and passed through a 70-µm filter. Cells were
886 resuspended for magnetic column enrichment (Miltenyi LD column depletion with streptavidin
887 microbeads and biotinylated antibodies against B220, Ter119, TCRbeta, CD3e). Cells were then
888 either processed directly for 10x single-cell analysis as reference sample or sorted by flow
889 cytometry for all live GFP+ cells. Cells were sorted into PBS with 0.04% bovine serum albumin

890 (BSA). Cell viability and counts were evaluated with Vi-CELL XR (Beckman Coulter), and samples
891 with viability >85% were used for sequencing.

892

893 For analysis, sequencing files were aligned to the mm10 mouse reference genome with the 10x
894 Genomics Cell Ranger (v3.1.0) count method using the default parameters. Raw count files were
895 then processed in Python (v3.9.7), removing doublets from each sample using Scrublet⁴⁹ with a
896 doublet score threshold of 0.3. Samples were merged and filtered, removing genes with no
897 counts, and retaining cells with 600 to 5,000 genes and 1,000 to 30,000 counts, leaving a total of
898 35,797 cells and 22,979 genes in the dataset. The raw counts were used to train a model of gene
899 expression using scvi-tools (v0.14.6) with each sample as a batch key. This model was used to
900 generate normalized expression values for all genes scaled to a library size of 100,000 and create
901 a tSNE representation of the data using Scanpy⁵⁰ (v1.8.2) with the default parameters. Leiden
902 clustering with a resolution of 0.8 gave 29 clusters which were assigned cell types after removing
903 three low quality clusters. For targeted analysis of JC, the data was subset on the three JC
904 clusters and a UMAP was created using Scanpy with a minimum distance of 0.5 and spread of 1.
905 Differential gene expression of JC clusters was performed using scvi-tools⁵¹, filtering on genes
906 with a bayes factor greater than 3, mean log fold change greater than 0, and proportion of cells
907 with non-zero expression greater than 0.1. The z-score of the average expression of the top 10
908 DE genes from each cluster was used for visualization. For low-dimensional embeddings of
909 feature plots, scVI normalized expression was used, clipping the top and bottom 1% of expression
910 values in the full dataset to the maximum and minimum of the color scale to prevent outliers from
911 skewing the visualization. To display expression of key features in dotplots, log-normalized and
912 scaled counts for each gene were averaged and standardized across cell types to have a value
913 ranging from 0 to 1.

914

915 **RNAscope**

916 Fresh-frozen spleen and lymph nodes were sectioned at 8um and then fixed overnight at 4°C in
917 10% neutral buffered formalin (Thermo Fisher Scientific, Waltham, MA) before proceeding with
918 an RNAscope RED 2.5 HD Chromogenic Assay kit (Advanced Cell Diagnostics, Newark, CA) for
919 detection of Aire mRNA. DapB probe was used as negative control and Polr2a probe was used
920 as positive control. Semi-quantitative scores were determined in a blinded fashion based on the
921 number of Aire⁺ cells per section.

922

923 **Integrin β_8 (ADWA-11) blocking Ab**

924 We injected IP 200ug of ADWA-11 into mice colonized with Hh for 7 days. On the same day we
925 adoptively transferred 100K CFSE-labeled naive Hh7-2 cells and tested their proliferation and
926 differentiation in the C1 MLN, 3 days after the transfer.

927

928 **Generation of bone marrow (BM) chimeric reconstituted mice**

929 To generate chimeric mice, 4-5 week old CD45.1 mice were irradiated twice with 500 rads/mouse
930 at an interval of 2-5 h (X-RAD 320 X-Ray Irradiator). A day after, bone marrow (BM) mononuclear
931 cells were isolated from donor mice, as indicated in each experiment, by flushing the femur bones.
932 Red blood cells were lysed with ACK Lysing Buffer, and lymphocytes were depleted for Thy1.2
933 using magnetic microbeads (Miltenyi). BM cells were resuspended in PBS and a total 3-4 x 10⁶
934 BM cells were injected intravenously into the irradiated mice. In case of mixed BMC reconstitution,
935 a ratio of 1:1 was used. Mice were kept for a week on broad spectrum antibiotics (1 mg/mL
936 sulfamethoxazole and 0.2 mg/ mL trimethoprim), followed by microbiome reconstitution by fecal
937 gavage. Mice were reconstituted for 1-2 months before Hh colonization. After 7 weeks, peripheral
938 blood samples were collected and analyzed by FACS 7 to check for reconstitution.

939

940 **Intravital multiphoton microscopy**

941 Naive Hh7-2 T cells were isolated from *Nur77-eGFP* Hh7-2tg mice, labeled with Cell tracker dye
942 (eBioscience Cell Proliferation Dye eFluor 450), and transferred into *mKate2-ON^{zbtb46};ROR γ t-eGFP* mice that had been colonized with Hh for 6 days. Fifteen hours following adoptive transfer
943 of Hh T cells, mice were euthanized and C1 MLN were immediately isolated and mounted in cold
944 RPMI with 10% FCS for intravital multiphoton microscopy. Image stacks were acquired with an
945 Olympus multiphoton FVMPE-RS system equipped with both InSight X3 and Mai Tai Deepsee
946 (Spectra-Physics) tunable Ti:Sapphire lasers. To acquire serial optical sections, a laser beam
947 (780 nm for eFluorTM 450 and 940 nm for simultaneous excitation of eGFP and mKate2) was
948 focused through a water immersion lens (N.A. 1.05; Olympus) and scanned with a field of view of
949 0.5 mm², at 600 Hz. Z-stacks were acquired in 2 mm steps to image a total depth of 150-200 mm
950 of tissue.

952

953 **Image analysis**

954 Raw image stacks were imported into Fiji (NIH) for T cell colocalization analysis. Provided images
955 are presented as a maximal projection of 3–6 mm optical sections. For visualizing individual
956 labelled cells expressing both the mKate2 and eGFP, the brightness and contrast were adjusted
957 accordingly to single positive green (eGFP) and red (mKate2) cells. Adoptively transferred Hh7-
958 2tg T cells were identified via positive labeling with cell proliferation dye eFluor 450. Primed Hh7-
959 2tg T cells were identified via expression of the *Nur77-eGFP* reporter. Cell identity was scored by
960 a combination of both fluorescent reporter expression as well as cell morphology. Specifically,
961 cells expressing mKate2 with a dendritic cell shape were scored as cDC, while cells expressing
962 both *ROR γ t-eGFP* and mKate2 (or eGFP alone) with an amoeboid (non-spherical) cell shape
963 were scored as ILC3. T cell interactions with cDC or ILC3 was strictly measured as direct (<1
964 micron) colocalization of cells with respective fluorescent and cell morphology combinations.

965

966 **Statistical analysis**

967 For animal studies, mutant and control groups did not always have similar standard deviations
968 and therefore an unpaired two-sided Welch's t-test was used. Error bars represent \pm s.d. Animal
969 sample size estimates were determined using power analysis (power = 90% and α = 0.05) based
970 on the mean and s.d. from our previous studies and/or pilot studies using 4–5 mice. No samples
971 were excluded from analysis. For analysis of ILC3 counts in MLN and LP of chimeric mice, a
972 paired two-sided t-test was used.

973

974 **Data availability**

975 Data generated for this project are available at the Gene Expression Omnibus with the accession
976 code GSE190372 and XXX. Published data GSE176282 was used for analysis.

977

978 **Code availability**

979 All code used for analysis in this manuscript is available at <https://github.com/nygctech/Kedmi->
980 CITEseq.

981

982 **Additional References**

983

984 39 Eberl, G. & Littman, D. R. Thymic origin of intestinal alphabeta T cells revealed by fate
985 mapping of RORgammat+ cells. *Science* **305**, 248-251, doi:10.1126/science.1096472
986 (2004).

987 40 Lochner, M. *et al.* In vivo equilibrium of proinflammatory IL-17+ and regulatory IL-10+
988 Foxp3+ RORgamma t+ T cells. *The Journal of experimental medicine* **205**, 1381-1393,
989 doi:10.1084/jem.20080034 (2008).

990 41 Kaplan, D. H., Jenison, M. C., Saeland, S., Shlomchik, W. D. & Shlomchik, M. J. Epidermal
991 langerhans cell-deficient mice develop enhanced contact hypersensitivity. *Immunity* **23**,
992 611-620, doi:10.1016/j.jimmuni.2005.10.008 (2005).

993 42 Dow, L. E. *et al.* Conditional reverse tet-transactivator mouse strains for the efficient
994 induction of TRE-regulated transgenes in mice. *PLoS One* **9**, e95236,
995 doi:10.1371/journal.pone.0095236 (2014).

996 43 Metzger, T. C. *et al.* Lineage tracing and cell ablation identify a post-Aire-expressing
997 thymic epithelial cell population. *Cell Rep* **5**, 166-179, doi:10.1016/j.celrep.2013.08.038
998 (2013).

999 44 Stoeckius, M. *et al.* Simultaneous epitope and transcriptome measurement in single
1000 cells. *Nat Methods* **14**, 865-868, doi:10.1038/nmeth.4380 (2017).

1001 45 Stoeckius, M. *et al.* Cell Hashing with barcoded antibodies enables multiplexing and
1002 doublet detection for single cell genomics. *Genome Biol* **19**, 224, doi:10.1186/s13059-
1003 018-1603-1 (2018).

1004 46 van Buggenum, J. A. *et al.* A covalent and cleavable antibody-DNA conjugation strategy
1005 for sensitive protein detection via immuno-PCR. *Sci Rep* **6**, 22675,
1006 doi:10.1038/srep22675 (2016).

1007 47 Hafemeister, C. & Satija, R. Normalization and variance stabilization of single-cell RNA-
1008 seq data using regularized negative binomial regression. *Genome Biol* **20**, 296,
1009 doi:10.1186/s13059-019-1874-1 (2019).

1010 48 Hao, Y. *et al.* Integrated analysis of multimodal single-cell data. *Cell* **184**, 3573-3587
1011 e3529, doi:10.1016/j.cell.2021.04.048 (2021).

1012 49 Wolock, S. L., Lopez, R. & Klein, A. M. Scrublet: Computational Identification of Cell
1013 Doublets in Single-Cell Transcriptomic Data. *Cell Syst* **8**, 281-291 e289,
1014 doi:10.1016/j.cels.2018.11.005 (2019).
1015 50 Wolf, F. A., Angerer, P. & Theis, F. J. SCANPY: large-scale single-cell gene expression data
1016 analysis. *Genome Biol* **19**, 15, doi:10.1186/s13059-017-1382-0 (2018).
1017 51 Lopez, R., Regier, J., Cole, M. B., Jordan, M. I. & Yosef, N. Deep generative modeling for
1018 single-cell transcriptomics. *Nat Methods* **15**, 1053-1058, doi:10.1038/s41592-018-0229-
1019 2 (2018).
1020